Paleoseismological and morphological evidence of slip rate variations along the North Tabriz fault (NW Iran)

Shahryar Solaymani Azad, Hervé Philip, Stéphane Dominguez, Khaled Hessami, Majid Shahpasandzadeh, Mohammad Foroutan, Hadi Tabassi, Michel Lamothe

▶ **To cite this version:**

HAL Id: hal-01089420

https://hal.sorbonne-universite.fr/hal-01089420v1

Submitted on 1 Dec 2014

Accepted Manuscript

Paleoseismological and morphological evidence of slip rate variations along the North Tabriz fault (NW Iran)

Shahryar Solaymani Azad, Hervé Philip, Stéphane Dominguez, Khaled Hessami, Majid Shahpasandzadeh, Mohammad Foroutan, Hadi Tabassi, Michel Lamothe

Please cite this article as: Azad, Shahryar Solaymani, Philip, Hervé, Dominguez, Stéphane, Hessami, Khaled, Shahpasandzadeh, Majid, Foroutan, Mohammad, Tabassi, Hadi, Lamothe, Michel, Paleoseismological and morphological evidence of slip rate variations along the North Tabriz fault (NW Iran), *Tectonophysics* (2014), doi: 10.1016/j.tecto.2014.11.010
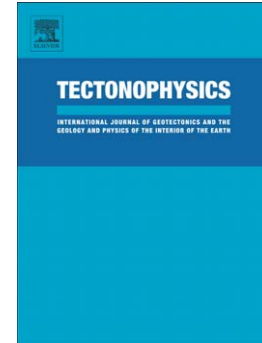
Paleoseismological and morphological evidence of slip rate variations along the North Tabriz fault (NW Iran)

Shahryar Solaymani Azad[1,2], Hervé Philip[2], Stéphane Dominguez[2], Khaled Hessami[3], Majid Shahpasandzadeh[4], Mohammad Foroutan[1,5], Hadi Tabassi[6], Michel Lamothe[7]

[1] Geological Survey of Iran, Seismotectonics and Seismology Department, P.O. Box: 13185 1494, Tehran, Iran

[2] Université Montpellier 2, Laboratoire Géosciences Montpellier, UMR CNRS 5243, Montpellier, 34095, France

[3] International Institute of Earthquake Engineering and Seismology (IIEES), Dibaji, 19531, Tehran, Iran

[4] Kerman Graduate University of Technology, Haftbagh Highway, Kerman, Iran

[5] Sorbonne Universités, UPMC Univ. Paris 06, UMR 7193, Institut des Sciences de la Terre de Paris (ISTeP), F-75005, Paris, France

[6] Ashtian Azad University, Ashtian, Iran

[7] Quebec University, P.O. Box: 8888, H3C 3P8, Canada

Corresponding author: S. SOLAYMANI AZAD, Geological Survey of Iran, Department of Seismotectonics and Seismology, P.O. Box: 13185 1494, Tehran, Iran;

shahryar.solaymani@gmail.com

Abstract

Northwest Iran is characterized by a high level of historical and instrumental seismicity related to the ongoing convergence between the Arabian and Eurasian plates. In this region, the main right-lateral strike-slip fault known as the North Tabriz fault (NTF) forms the central portion of a large crustal fault system called the Tabriz fault system (TFS). The NTF is a major seismic source along which at least three strong and destructive earthquakes have occurred since 858 AD. The two most recent destructive seismic events occurred in 1721 AD and 1780 AD, rupturing the SE and NW fault segments, respectively. This paper reports paleoseismological and quantitative geomorphologic investigations on the SE segment of the NTF, between the cities of Bostanabad and Tabriz. These observations help to improve our understanding of the seismic hazard for Tabriz city and its surrounding areas. Our field investigations revealed evidence of successive faulting events since the Late Quaternary. Paleoseismic investigations indicate that since 33.5 kyr, the SE segment of the NTF has experienced at least three major (M>7.5) seismic events, including the 1721 AD earthquake (M=7.6–7.7). Along the NW segment of the fault, however, our results suggest that the amount of strong (M~7.5) seismic events during the same period is significantly greater than along the SE segment. One possible explanation of such a difference in seismic activity is that the Late Quaternary-Holocene coseismic slip rate is decreasing along the NTF from the northwest to the southeast. This explanation contradicts the former hypothesis of a constant slip rate along the whole length of the NTF. In addition, more distributed deformation along several parallel fault branches, in a wider fault zone of the SE segment of the NTF may be considered as additional evidence for the estimation of lower rate of deformation along the fault segment. Such a slip distribution pattern can explain the existence of smaller (~300 m) Pliocene-Quaternary cumulative dextral offsets along the SE fault segment than the measured cumulative offsets along the NW segment (~800 m) of the NTF.

1.   Introduction

The Iranian plateau forms the central portion of the Alpine–Himalayan orogenic belt (e.g. Sengör and Kidd, 1979; Sengör and Yilmaz, 1981; Jackson and McKenzie, 1984; Jackson, 1992). Its large-scale topography and regional surface morphology both resulted from the Eocene to Miocene collision and ongoing convergence between the Arabian plate to the south and the Eurasian plate to the north. Global positioning system (GPS) measurements (Nilforoushan et al., 2003; Vernant et al., 2004) reveal that present-day northward motion of the Arabian plate relative to the Eurasian plate is about 20 to 25 mm yr^{-1}.

In western Iran (between 45°E and 54°E), the Arabia–Eurasia convergence is mainly accommodated by crustal deformation localized on both the northern and southern sides of Central Iran, which is commonly described as a more rigid portion of the Iranian plateau (e.g. Stöcklin 1968 and 1974; Jackson and McKenzie, 1984). However, recent paleoseismic studies have documented the occurrence of several large-magnitude earthquakes along the prominent strike-slip faults slicing Central Iran indicating it does not behave totally as a rigid block (Foroutan et al., 2012, 2014). On the southern side of Central Iran, along the Zagros ranges, the rate of microseismicity is high (e.g. Berberian, 1995; Oveisi et al., 2008), but large seismic events are relatively rare and occur at depths ranging between 8 and ~30 km, and mostly reported without surface faulting (e.g. Maggi et al., 2000; Talebian and Jackson, 2004; Tatar et al., 2004; Oveisi et al., 2008; Nissen et al., 2011). On the northern side of Central

3

Iran, despite a lower rate of instrumental seismicity, the region including southern Armenia–eastern Turkey and northwestern Iran–Transcaucasian territories has experienced large and destructive historical earthquakes (e.g. Berberian, 1997; Cisternas and Philip, 1997) (Fig. 1). In this framework, most of the earthquake hypocenters are shallow (e.g. Siahkali Moradi et al., 2011) and commonly associated with surface faulting (e.g. Berberian and Yeats, 1999; Hessami et al., 2003a; Karakhanian et al., 2004). Considering their large magnitudes and long return periods, these earthquakes can be interpreted as typical intra-plate seismic events (e.g. Berberian and Yeats, 1999). According to the amount of seismic moment released by earthquakes within E Turkey and NW Iran, tectonic deformation in the region is almost totally accommodated by coseismic slip (e.g. Jackson and Ambraseys, 1997). Because of these characteristics, the region of NW Iran, characterized by a dense population, is clearly subjected to a high level of seismic hazard and risk as well. However, in some cases (e.g. 1988 Spitak earthquake in Armenia, M ~6.7) the level of seismic hazard was underestimated by previous seismic hazard analysis (Berberian, 1997). During the last three decades, many researchers (e.g. Berberian and Arshadi, 1976; Hempton and Dewey, 1983; Berberian, 1997; Cisternas and Philip, 1997; Avagian, 2001; Karakhanian et al., 2002; Jackson et al., 2002; Hessami et al., 2003a; Karakhanian et al., 2004; Davtian, 2007; Solaymani Azad, 2009) have performed active tectonic and paleoseismological studies to improve the seismic hazard assessment within this intra-plate region. The occurrence of strong earthquakes, long quiescent times, and intensely active periods (temporal seismic clustering) are the main characteristics of this active region. In the Iranian part of the region, most active tectonic studies have focused on the North Tabriz fault (NTF) as a well-known seismic source in the area (e.g. Berberian and Arshadi, 1976; Hessami et al., 2003a).

Hessami et al. (2003) performed the first paleoseismological study on the NW segment of the NTF to characterize both its kinematics and seismic behavior. Their study revealed that the

NW segment of the NTF has ruptured at least during four large earthquakes, since 3600 BP, with a mean recurrence interval of 820±170 years, including the most recent one in 1780 AD. The return period of strong earthquakes along the entire length of the fault is still to be assessed; nevertheless, these results clearly indicate that the seismic risk for the city of Tabriz and its surrounding regions is increasing to a very high level (e.g. Copley and Jackson, 2006). Unfortunately, the rapid development of the Tabriz region, in terms of industry, population, and urban extension, is exacerbating the situation. Despite the significance of the issue, the first-order kinematic and behavioral characteristics of the NTF are still debated, and the fault segmentation model, short- and long-term seismologic behavior, and kinematics of the fault are all still undetermined. In this context, a detailed study along the SE segment of the NTF is essential to better determine the regional seismic hazard.

To achieve our aim of improving seismic hazard assessment in the region, we performed morphotectonic and paleoseismological investigations along the SE segment of the fault, for which almost no data were available. The results of our systematic morphotectonic, seismotectonic and paleoseismological field investigations (see Solaymani Azad, 2009) complemented those of earlier seismotectonic and paleoseismological studies along the NW segment of the NTF (Karakhanian et al., 2002, 2004; Hessami et al., 2003a). In the following sections, we discuss first the distribution of both cumulative and coseismic deformations along the NTF, and then outline the accommodation of deformation on the NW and SE fault terminations. All these data and derived results are used to better constrain the seismologic behavior of the fault such as the maximum magnitude, slip per event, and recurrence time for each segment in order to improve the assessment of seismic hazard for the city of Tabriz and its surrounding areas. These results also increase our understanding of the present-day geodynamics of NW Iran.

2.   Tectonic setting

NW Iran is situated in the central part of the Arabia–Eurasia collision zone where crustal deformation has been dominated since the Late Miocene by a N–S shortening associated with an E–W extension (e.g. Berberian, 1981, 1997; Cisternas and Philip, 1997; Karakhanian et al., 2002, 2004; Copley and Jackson, 2006). This mainly strike-slip stress field has caused prominent faulting accompanied by strong earthquakes, and controls the distribution of recent volcanoes (Fig. 1). Based on geodetic measurements and numerical modeling (Vernant and Chéry, 2006), strain rates reach ~7 mm yr^{-1} in Zagros and ~13 mm yr^{-1} between Central Iran and Eurasia. At the northernmost boundary of the collision, most of the convergence is accommodated in the Caucasus and the Kura foreland basin, which undergo a N–S contraction (e.g. Philip et al., 1989; Priestley et al., 1994; Philip et al., 2001; Copley and Jackson, 2006; Forte et al., 2010). In NW Iran, however, a considerable right-lateral slip rate of ~8 mm yr^{-1} has been measured. Based on the GPS measurements (e.g. Masson et al., 2006; Vernant and Chéry, 2006; Reilinger et al., 2006), a large portion of this right-lateral strike-slip movement is localized along the NTF, as well as along the Guilato-Siahcheshmeh-Khoy fault (GSKF) system (Fig. 1). Berberian (1997) and Karakhanian et al. (2004) suggested that the NW–SE striking NTF can be considered as the eastern prolongation of the GSKF. According to some authors (e.g. Barka and Kandinsky-Cade, 1988; Westaway, 1990; Barka, 1992; Jackson, 1992), these two fault zones transfer the right-lateral movements of the North Anatolian fault toward the east, although they are not connected to each other.

Early studies considered the NTF as a major tectonic structure that has been inherited at least from Early Paleozoic and controls the distribution of geological formations and facies since Paleozoic (e.g. Eftekhar Nezhad, 1975; Nabavi, 1976; Berberian and Arshadi, 1976). Nabavi

6

(1976) noticed that Devonian and Carboniferous formations are missing on the southern block of the fault, implying that the NTF was the northern limit of the Iranian Caledonian paleorelief.

The NTF strikes N135°E over a length of more than 120 km, from the northwest of Sufian to the southeast of Bostanabad (Fig. 2). The fault trace is not continuous and consists of several strands that make up the two main NW and SE fault segments, as established by previous authors (e.g. Karakhanian et al., 2004). Due to repeated earthquake ruptures, the NTF has a clear surface expression along most of its trace and exhibits convincing geomorphic evidence of recent activity. Right-lateral strike-slip movements along the NTF were first documented by Nabavi (1976) based on a study of geological offsets. Next, Berberian and Arshadi (1976) identified right-lateral offsets through the interpretation of aerial photographs. Since then, more detailed morphotectonic investigations have been carried out on the related geomorphic features by several researchers (Berberian, 1997; Karakhanian et al., 2002, 2004; Hessami et al., 2003a; Hessami and Jamali, 2008; Solaymani Azad, 2009; Fathian Baneh et al., 2011). Based on the interseismic geodetic GPS measurements in NW Iran (e.g. Masson et al., 2006; Vernant and Chéry, 2006), the present-day slip rate (averaged over a few years) of the NTF could reach 5-8 mm yr^{-1}. This estimation is higher than the geological slip rate of ~2 mm yr^{-1} inferred over the Holocene along the NW segment of the NTF (Karakhanian et al., 2004). However, the geodetic slip rates remain consistent with the Late Quaternary slip rates of 3.1–6.4 mm yr^{-1} (Hessami et al., 2003a) and ~7 mm yr^{-1} (Rizza et al., 2013) along the same segment of the NTF.

The NW and SE terminations of the NTF are marked by the Mishu and Bozghush ranges, respectively (Figs. 1 and 2). These roughly E–W trending ranges have almost similar dimensions of 85×25 km and average altitudes of ~3000 m above sea level. The Mishu and

7

Bozghush ranges are bordered by several oblique and reverse E–W faults that join to the NTF (Fig. 2).

3. Historical and instrumental seismicity

Historical seismic records in NW Iran show that the Tabriz region has experienced intense seismic activity during the last centuries (e.g. Ambraseys, 1978; Ambraseys and Melville, 1982; Berberian, 1994; Berberian, 1997; Berberian and Yeats, 1999; Karakhanian et al., 2004; see Table 1). Moreover, the NTF ruptured by several destructive and tragic earthquakes during the past millennium (e.g. Ambraseys and Melville, 1982; Berberian, 1997; Berberian and Yeats, 1999). The NTF, whose trace crosses Tabriz city, can be considered as the main seismic source for this area.

Since 858 AD, Tabriz city has experienced at least 12 destructive seismic events, in 858, 1042, 1273, 1304, 1550, 1641, 1650, 1657, 1664, 1717, 1721, and 1780 AD (e.g. Ambraseys and Melville, 1982). The occurrence of large (M>7.0) earthquakes of 1042 AD, 1721 AD, and 1780 AD, were associated with the NTF and produced clear surface ruptures (Ambraseys and Melville, 1982; Berberian, 1997; Berberian and Yeats, 1999; Hessami et al., 2003a). The five destructive earthquakes of Sarab (1593 AD), SE Tabriz (1721 AD), NW Tabriz (1780 AD), Marand (1786 AD), and Tassuj (1807 AD) reveal a seismic migration from the southeast toward the northwest over a period of 214 years (Fig. 2). While this pattern of strain release could correspond to earthquake clustering, as suggested by some authors (e.g. Kagan and Jackson, 1991; Berberian, 1997; Karakhanian et al., 2004), it could also reveal interactions of structural fault segments of the Tabriz fault system (TFS).

Since 1780 AD, the NTF has remained seismically silent, a period of quiescence of more than two centuries. However, recent seismological studies along the fault show the occurrence of numerous shallow microseismic events limited to depths of 7–21 km (Siahkali Moradi, 2008; Siahkali Moradi et al., 2011).

4.   Geomorphology and kinematics of the NTF

Within the arid to semi-arid territory of Persia, erosion rate over the Quaternary time period is low, generally less than 3 m Ma-1 (Le Dortz et al., 2011; Shabanian et al., 2012). Hence, the down-cutting rate of incising stream channels or seasonal rivers is low. Moreover, taking into consideration that the NTF, especially within the Tabriz region is a primary strike-slip fault, the uplift rate is much less than the horizontal slip rate and it remains insignificant along the fault. Morphologically, there is no then very sharp difference between young and younger/old and older adjacent stream channels. Since there is not adequate absolute dating on the geomorphic offset features along the whole length of the NTF, the relative age of the observed offset features has been verified during the field investigations. In addition, qualitative roughness comparisons between the abandoned alluvial fan surfaces that are hosted the offset features provide supplementary evidence on the relative age of the offset features, which are compatible with Frankel and Dolan's (2007) observations.

The occurrence of repeated surface–faulting events along the NTF produced convincing geomorphic evidence of its recent activity. Variations in the seismic behavior of the fault during the historical time (e.g., the successive seismic events of 1593 AD to 1807 AD) (Fig. 2), kinematics of faulting, geomorphology and geometry of the fault scarps and also the

distribution of coseismic ruptures along the NTF lead us to discuss the NTF in the framework of the TFS. The TFS can be divided into three structural portions: a central sector dominated by strike-slip movements and two reverse, oblique-slip sectors at either ends.

4.1. The Northwestern sector of the TFS

The NW sector of the TFS corresponds to the Mishu range (Figs. 1 and 2). The Mishu range is composed of Proterozoic igneous rocks (granite, rhyolite, and gabbro), separated on both sides from Neogene rocks by the Tassuj, North Mishu, and South Mishu faults. Farther south, the Sufian and Shabestar faults, parallel to the South Mishu fault, separate Neogene rocks from Quaternary alluvial fan deposits. All of these E–W striking faults have a pure or reverse oblique with a right-lateral component, and merge together west of Sufian city (Figs. 1 and 2). N–S active compression is evidenced west of Marand city by a large E–W Quaternary fold, which shows a clear antecedent stream pattern (Fig. 3). Southwest of the fold, geomorphic evidence of dextral strike-slip faulting along the North Mishu fault is observed. These features are compatible with slip partitioning along this portion of the TFS. The Mishu range can be considered, then, as a compressional fault relay zone that absorbs a part of the displacement along the NW right-lateral strike-slip segment of the NTF. Thus, the seismic events of 1786 AD and 1807 AD that occurred along the Mishu range should be interpreted as thrust or oblique-slip events.

4.2. The central sector of the TFS

This central sector of the TFS is the main strike-slip zone of the fault system that was called the NTF in early studies (e.g. Berberian and Arshadi, 1976). Based on the fault characteristics

10

such as its geomorphology and geometry (Karakhanian et al., 2002, 2004), the distribution of historical seismic ruptures (Ambraseys and Melville, 1982; Berberian and Yeats, 1999), and pre-historical seismic records (Hessami et al., 2003a; Solaymani Azad, 2009), the NTF can be divided into two major fault segments: the NW and the SE segments, with a right-stepping pattern (Fig. 4). Karakhanian et al. (2004) showed that the main overlapping zone between the NW and SE fault segments of the NTF corresponds to a large pull-apart basin in which Tabriz city is situated (Fig. 4). Within the pull-apart basin, the morphology of fault scarps is mainly controlled by the variations in the vertical slip component of NNW-striking normal faults.

The NW segment of the NTF strikes N120-130°E and has a length of ~50 km. The western part of the fault segment extends from Sufian city, follows the southern flank of the Mero range, and ends at the northeastern boundary of Tabriz city (Fig. 4). The most recent coseismic surface faulting (1780 AD) along this portion of the TFS permits an easy observation of the fault trace (Fig. 4). A maximum cumulative right-lateral offset of 256 m was documented by Hessami et al. (2003a) along this segment of the NTF. Our interpretation of aerial photos and field observations, however, show that the cumulative dextral offset in the Pliocene-Quaternary units (Eftekhar Nezhad, 1993) near Khajeh-Marjan village is significantly larger, reaching about 500 m, which have been preserved on intermittent streams and alluvial fans (Fig. 5). Farther to the east, a horizontal geomorphic offset of 800 m has been preserved within the Pliocene-Quaternary alluvial fans (Eftekhar Nezhad, 1993) (Fig. 5). This offset feature represents the largest cumulative displacement measured along the fault segment over the Pliocene-Quaternary time period.

The minimum horizontal geological slip rate along the NW segment of the NTF amounts to about 2 mm yr^{-1} (Karakhanian et al., 2004). Accounting for the slip rate of 5–7 mm yr^{-1} derived from both the geomorphic (Hessami et al., 2003a; Rizza et al., 2013) and geodetic

11

(Masson et al., 2006; Vernant and Chéry, 2006) measurements, the right-lateral offsets of 500 and 800 m would be accumulated over the last 70 to 114 kyr, respectively. The maximum cumulative geological offset has been reported by Nabavi (1976) between the Mishu and Mero ranges and amounts to 20–25 km (based on our measurement). If the Quaternary slip rate (~5 mm yr^{-1}) along the NW segment of the NTF has remained constant over the last million years, this maximum cumulative geological offset may indicate the onset of the right-lateral strike-slip faulting along the NTF at 4–5 Myr ago (during the Early Pliocene). This age estimate agrees with the initiation of the North Anatolian fault propagation proposed by Barka and Kandinsky-Cade (1988) and Barka (1992), which is in turn coeval with the expulsion of the Anatolian block and NW Iran toward the west and east, respectively (diachronously after the closing of the Neothetys) (Philip et al., 1989; Cisternas and Philip, 1997; Philip et al., 2001).

The smallest dextral geomorphic offset observed along the NW segment of the NTF amounts to about 4–5 m (Hessami et al., 2003a). This smallest preserved offset can be produced by an earthquake as large as M~7.5 (using Wells and Coppersmith's [1994] relationship). This is consistent with the paleosismic observations along some other seismogenic fault zones within the Transcaucasian region such as the North Anatolian fault (e.g. Rockwell et al., 2009; Meghraoui et al., 2012).

The second segment of the central portion of the TFS has an average strike of N135-145°E and a length of 60 km. It extends from the Tabriz pull-apart basin to the southeast of Bostanabad city, following the northeast flank of the Sahand strato-volcano (Fig. 4). This southeast prolongation of the NTF was initially proposed by Ambraseys and Melville (1982) while considering the location of the surface rupture associated with the 1721 seismic event. At least three right-stepped branches can be observed along the SE segment of the NTF. These branches of the main strike-slip fault segment create two right steps, one west of

Ghurugol lake and another west of the Shebli village (Figs. 4 and 6). Moreover, several secondary branches can be identified on both sides of the main fault over a zone of ~2 km wide. The deformation zone appears more diffuse than the NW segment of the NTF, where seismic slip concentrates on a narrower fault zone (Fig. 4). To the west of Ghurugol lake, there is clear evidence of active dextral faulting associated with a slight normal component (Fig. 6d). Normal faulting within this area (around the village of Shebli) was previously reported by Berberian and Arshadi (1976). Most likely, this secondary normal slip component that observed along the main right-lateral strike-slip faulting zone can be a local feature caused by the right-stepping geometry of the fault branches (Fig. 6).

Aerial photographs and field studies reveal that Ghurugol lake is likely a pull-apart basin formed between the two right-stepped, en-echelon branches of the SE segment of the NTF (Fig. 6). In addition, the change in stream direction observed on the northern side of the lake (most probably due to active uplift and faulting) has possibly contributed to formation of this lake. East of the lake, there are several dextral offset features that imply repeated occurrences of coseismic surface faulting. There, the mean value of the maximum Pliocene-Quaternary (Eftekhar Nezhad, 1993) cumulative dextral offset is about 300 m (Figs. 6a, 6b, and 8).

Results of recent morphotectonic studies and aerial photograph interpretations by Hessami and Jamali (2008) and Fathian Baneh et al. (2011) reveal two cumulative dextral offset rivers where the NW and SE segments of the NTF overlap. The amounts of maximum cumulative dextral offset of the rivers vary between 1100 m (Hessami and Jamali, 2008) and 1170 m (Fathian Baneh et al., 2011) within the Pliocene-Quaternary materials. Interestingly, the value of 1100 m dextral offset documented in the overlap zone is compatible with the sum of the 800 m and 300 m maximum cumulative dextral Quaternary offsets observed along the NW and SE segments, respectively.

East of Ghurugol lake (12 km west of Bostanabad), the fault zone widens to more than 1500 m. There, three sub-parallel fault branches, labeled I, II, and III, can be identified (Figs. 6a and 6b). The northern one (branch I) clearly cuts the surface morphology, indicating recent activity (Fig. 6e). 1 km farther south, the fault branch II corresponds to the main fault trace with a pure right-lateral strike-slip component (Figs. 6a and 6b). The amount of Quaternary offset features such as streams and ridges vary from ~7 to 300 m along this fault (Fig. 6). In both satellite images and aerial photographs, this branch extends between the southeast of Bostanabad city (to the SE) and the Ghurugol lake to the northwest (Fig. 4). The southern fault (branch III) is approximately situated 150 m to the south of branch II. The geomorphology of the fault scarp is compatible with a NE-dipping reverse to thrust fault. The fault strike (N140-145°E) is slightly oblique to the central branch II, as illustrated in Fig. 6.

4.3.   The Southeastern sector of the TFS

The SE prolongation of the NTF terminates in the southeast of Bostanabad, where the fault divides into two branches. The main strand strikes gradually eastward and follows the southern flank of the Bozghush range. The second branch continues in scattered form 65 km toward the southeast in the Qara Chiman direction (Fig. 2). Field observations 30 km southeast of Bostanabad reveal geological evidence of a NW-striking fault zone, which could be associated with the moderate seismic event in 1965 AD (M=5.1, I0=VII; Ambraseys and Melville, 1982).

In the context of geomorphology, the SE portion of the TFS is associated with a fault network affecting the Bozghush range, including the South Bozghush fault to the south and the North Bozghush, South Sarab, and Duzduzan faults to the north (Berberian, 1997; Solaymani Azad, 2009) (Fig. 2). The South and North Bozghush faults separate the Eocene volcanic rocks of

the Bozghush range from Neogene and Quaternary deposits. Farther north, the South Sarab and Duzduzan faults (parallel to the North Bozghush fault) affect Quaternary alluvial fan deposits. These faults are generally E-striking, dip-slip reverse or oblique-slip reverse-dextral faults. The Bozghush range corresponds to a large antiform structure mainly composed of Eocene volcanics (trachyandesite and lava flows). Field observations indicate that the E–W longitudinal depression on top of the Bozghush range corresponds to a graben, which is essentially related to extrados extension (Fig. 7).

The seismic event of 1593 AD that occurred in the Sarab region could be assigned to the faults bounding the northern flank of the Bozghush range (Fig. 2). Later, in 1844 AD and 1879 AD, other destructive seismic events occurred along a NE-striking fault zone on the eastern side of the range (Ambraseys and Melville, 1982; Hessami et al., 2003b; see Fig. 1).

4.4. Pattern of active deformation along the TFS

Our observations indicate that the amount of maximum Pliocene-Quaternary cumulative dextral offset varies along the three sectors of the fault system outlined above. The offset values range from 300 m to ~800 m for the east and west central sectors, respectively. However, smaller lateral offsets and more frequent reverse faulting features are preserved along the northwestern and southeastern sectors of the fault system. We suggest that the horizontal component of displacements along the NW and SE segments of the NTF are absorbed within the Mishu and Bozghush ranges as two fault terminations. Both the sharpness and multiplicity of the similar Pliocene-Quaternary cumulative offsets along the central sector of the TFS (i.e., the NW and SE segments of the NTF) suggest that these offsets have accrued through large earthquakes rather than by interseismic creeping. Moreover, the time periods in which the maximum dextral offsets were accumulated may not necessarily be the same; i.e.,

different cumulative offsets do not necessarily indicate different slip rates. Thus, the paleoseismological studies have been performed to investigate the possibility of slip rate variations along these portions of the fault system, and to investigate the seismic behavior of the SE segment of the NTF.

5. Paleoseismological study along the SE segment of the NTF

The SE segment of the NTF is known to have ruptured during the 1721 AD Tabriz earthquake (Ambraseys and Melville, 1982; Berberian, 1997; Berberian and Yeats, 1999). This earthquake is the most recent macroseismic event along the SE fault segment that severely damaged the Tabriz metropolitan area and its surroundings, including the cities of Shebli and Bostanabad (Figs. 1, 2, and 4).

The best-preserved surface expression of geomorphic and structural features along the fault segment is found around Ghurugol lake. In this area, the fault zone exhibits clear geomorphic evidence of repeated dextral coseismic surface ruptures such as beheaded streams and shutter ridges within the meizoseismal area of the 1721 AD earthquake (Figs. 2, 6 and 8). The fault cuts through the Late Quaternary deposits at the southern piedmont of a range made of Eocene volcanics and several river channels trending normal to the fault strike (Figs. 6 and 8). Streambeds, gullies, and ridges are systematically offset along the main fault trace (Figs. 6, 8, and 9). These features make the area a suitable site for paleoseismological trenching and enable detailed quantitative geomorphic measurements. The clearest feature is a recent channel located between Ghurugol lake and Bostanabad, which was right-laterally offset by 7±1 m (Fig. 9b). This offset could be produced either by a strong earthquake of magnitude

M~7.7 (according to Wells and Coppersmith's [1994] relationship) or by two or more smaller seismic events. Taking into consideration the ~7 m dextral offsets remain as the smallest well-preserved offset features that are seen along the SE segment of the NTF, these offsets should more likely correspond to the occurrence of a single strong earthquake.

Farther northwest, several offset streams provide evidence for cumulative offsets produced by several incremental seismic events. Various amounts of cumulative dextral offsets (~7, 45, 105, 150, 250, and 300 m) were measured along this segment of the NTF. The maximum 300 m dextral offset is restored through satellite images and aerial photographs by matching the streams and ridges on both sides of the fault trace (Figs. 6 and 8).

Along this portion of the fault segment, the vertical component of cumulative displacements varies between 5 and 10 m, but in all cases either the dip-slip component is subsidiary to the main right-lateral strike-slip movement or it corresponds to slip on secondary dip-slip fault branches close to the main strike-slip fault. At first glance, the southern block seems systematically down-thrown relative to the north side, while strike-slip movement along the fault created scarps facing both to the north and south as a result of the lateral offset of topography (Fig. 8c).

West of Bostanabad, faulting is distributed along at least three N135°E, roughly, parallel fault branches. However, nearly pure right-lateral strike-slip faulting and more recent deformation are localized along the main fault trace of the NTF (section 4.2; see also Figs. 6 and 8). At this location, our investigations focus on two sites along the main fault branch; hereafter referred to as sites 1 and 2 (Fig. 8b). At sites 1 and 2, three trenches (T1, T1bis, and T3) were excavated across the main dextral fault branch and a single trench (T2) was excavated across the southern thrust fault branch. Results are discussed in the sections 5.1 and 5.2 below.

17

5.1. Site 1

This site is located 1.2 km east of the Ghurugol lake, where the NTF zone cuts the well-developed Quaternary alluvial fans that overlie the southern flank of a range, composed of Eocene volcanics, parallel to the fault trace (Figs. 6 and 8). Farther south, these alluvial fans are dammed by several hills associated with large shutter ridges (Fig. 8).

Some of these shutter ridges (especially to the east) are constituted by Eocene volcanic rocks, while other hills toward the west are formed by younger (Pliocene-Quaternary) sedimentary units. In a quarry trench within the western hill, we observed considerable Quaternary deformation in the alluvial fan deposits. This alluvium, which was deposited unconformably over the Miocene-Pliocene volcano-detritic units of the Sahand volcano, was folded and faulted between the main-dextral (branch II in section 4.2) and the secondary-reverse (branch III in section 4.2) fault branches (Fig. 10), indicating a local transpressional tectonic regime.

To select suitable places to conduct paleoseismic studies, we first used large-scale digital elevation models (DEMs) extracted from differential global positioning system (DGPS) surveying. In addition, the detailed DEMs together with our field investigations allowed us to better determine the surface geometry of the fault branches and the related fold geometry (Fig. 11).

Along the main fault trace, we found several offset markers indicating recent horizontal movements with typical offsets of ~7 m that may correspond to the occurrence of the most recent seismic event (Fig. 9).

5.1.1. T1bis and T1 Trenches

Site 1 is located on the main dextral fault branch of the SE segment (Figs. 8, 10, and 11). We excavated two trenches, T1bis and T1, 4 m apart and perpendicular to the fault trace. These two trenches were 13 and 15 m in length, respectively, and ~4 m in depth (Figs. 12 and 13). Within these trenches, the bedrock to the south is sheared and thrust over younger deposits to the north along a 7–8 m wide fault zone (Figs. 12 and 13).

5.1.1.1. Trench stratigraphy of T1bis and T1

Unit 1: This unit corresponds to an undifferentiated Miocene-Pliocene formation including a 3–5 m wide fault breccia (unit 1a) situated near to the main fault plane (unit 1b). It constitutes the basement of the southern compartment of the fault zone (Figs. 12 and 13).

Unit 2: This unit is located on the northern compartment of the fault zone. It is mainly composed of non-stratified light ochre silty-clay and carbonate lake sediments (unit 2a). No organic material was found in this unit. This unit contains very well-preserved seismites generated by paleo-earthquakes. These structures, which are currently buried at a depth of 1–2.5 m, correspond to flame-form distribution of liquefaction features made of sandy-silty materials coming from the lower part of unit 2 and lower layers (Figs. 12, 13, and 14).

Based on these observations, we conclude that unit 2 is a sag pond deposit (lake sediments) close to the fault zone that was mainly composed of saturated, unconsolidated, sandy-silty materials that were subjected to liquefaction during earthquake(s). According to required pore-water pressure, overburden thickness, soil density, and soil porosity for occurrence of liquefaction (e.g. Ishihara, 1974; Bertero et al., 1994), this unit could be affected by generation of liquefaction at a depth of 10-20 m. Taking into consideration that the sag pond deposits are covered by soils that are not affected by these seismites (Figs. 12, 13, and 14), it

appears that the liquefaction features are older, and therefore cannot be associated with the most recent earthquake (1721 AD).

Unit 2b, south side of the unit 2a, is composed of colluvial deposits. The clasts of this unit originate from the southern compartment while the matrix was comprised mainly of fine sag pond deposits from the northern compartment. Because elements of unit 2a appear inter-fingered with unit 2b, we interpret unit 2b as a lateral sedimentary variation of the sag pond deposits (Fig. 15). It must be noted that the age of the base of this colluvial subunit (2b) varies laterally, from north to south. Within unit 2, the isochrones are most probably subhorizontal rather than oblique. This observation is very important for the interpretation of seismic events in trenches T1bis and T1. Recently, unit 2 has been successively cut by faulting events of the main fault zone between meters 4–5.5 and 5.5–7 in trenches T1bis and T1, respectively (Figs. 12 and 13). It is in fact the earliest recognized post-event horizon for one or stack of several seismic events on the T1bis and T1 trench walls (Fig. 15).

Unit 3: This unit corresponds to an unconsolidated and well-washed grayish graded-bedding deposit associated with the infilling of a paleo-gully. The gully is localized within the main fault zone in a graben bounded by two fault planes (between meters 4.7 and 5.5 in Fig. 12). Surface ruptures of the more recent seismic events have affected this unit.

Unit 4: This unit consists of a dark, developed paleosol that covers unit 2 conformably. This unit mainly contains fine organic materials, fossil roots, and rare clastic elements, indicating the sag pond depositional conditions lasted until the formation of this paleosol.

Unit 5: This unit corresponds to a brown superficial soil that contains organic material, sand, and numerous pebbles. This unit aggraded on an erosion surface that is incised into unit 2 (meter 0.5 in the T1bis trench, Fig 12).

Unit 6: This unit is the most superficial (youngest) one and composed of fine-grained modern soil to the north (unit 6a) and a colluvium to the south (unit 6b) that contains a considerable fraction of organic material. The upper part of the unit 6 has been partly reworked by recent agricultural activities.

5.1.1.2.   Fault planes on the T1bis and T1 trench walls

On the trench walls, several fault planes are clearly visible (Figs. 12 and 13). Generally, the fault planes consist of south-dipping thrusts that become rapidly vertical at depth. Some of these fault strands crosscut the youngest sediments and related to the occurrence of the most recent earthquake (i.e. units 5 and 6), and the others are older since they are sealed by these young units (meter 7 in the T1bis trench). The main fault (between meters 3 and 4 in the T1bis trench) consists of a 50-cm wide subvertical shear zone. This zone is limited on both sides by steep planes that cut the young units. The southern one clearly reaches the surface (meter 4 in T1bis and meter 6 in T1), as shown in Figs. 12 and 13.

5.1.2.   T2 trench

We dug the third trench (T2) at site 1, just across the thrust fault scarp, 140 m south of the first and second trenches (T1bis and T1) (Figs. 8, 11, and 16). This trench has a length of 8 m and depth of 2.5 m.

5.1.2.1.   Trench stratigraphy of T2

21

Unit 1: This unit is composed of deformed Miocene-Pliocene sediments and includes generally two subunits: a faulted one localized in 20–30 cm-wide shear zone (unit 1a), and the other one which is situated in the northern compartment of the fault zone (unit 1b) (Fig. 16).

Unit 2: This unit consists of a gray consolidated colluvial deposit which contains fine elements as a matrix with carbonate impregnations. Some fossil root traces associated with the paleosol of unit 4 (below) are visible at the top of this unit. Some gravels are also present. This unit unconformably overlies the Miocene-Pliocene bedrock (unit 1) with a very well-developed erosional surface (Fig. 16). This unit exists only on the hanging wall of the fault.

Unit 3: This unit corresponds to a well-stratified alluvial fan deposit hardened by carbonated impregnations. The unit contains cobbles that are inter-bedded with fine sandy strata. Bedding dips gently (about 10°) northward.

Unit 4: This unit is a reddish-brown partially hardened paleosol. It contains organic material and fine vertical carbonate lodes, which probably correspond to fossil root traces. Like unit 2, this unit exists only on the hanging wall of the fault.

Unit 5: This unit is a grain-supported colluvial wedge formed at the immediate vicinity of the superficial trace of the fault. It contains cobbles and some pebbles with a loose matrix. This colluvial wedge is clearly cut by the fault.

Unit 6: This unit corresponds to a colluvial wedge that overlaps unit 5. This unit contains reworked materials from unit 4.

Unit 7: This unit corresponds to the modern soil, rich in organic material. It has been partially reworked by recent agricultural activity.

5.1.2.2. Fault planes on the T2 trench wall

As mentioned before, the fault scarp is formed by a low angle fault and shows clear morphologic evidence of a reverse component (see section 4.2). Once the trench was excavated, a thrust fault plane appeared dipping (33°) to the northeast (Fig. 16). In this trench, the deformation is concentrated along a narrow (20–30 cm wide) shear zone. The fault plane cuts the uppermost ground units (such as unit 5), indicating a very recent activity, most probably coeval with a large slip event on the main strike-slip fault.

5.2. Site 2

About 1.4 km farther east of site 1, an east-facing artificial riser (made for agricultural purposes) provides another outcrop of the NTF. This outcrop is located just west of an offset riverbed (Figs. 8a and 8b). Here, the main fault zone is composed of a narrow steep shear zone cutting through the Quaternary fan deposits to the south and Neogene bedrock to the north that is capped by a very young soil unit (Fig. 17).

Sedimentary units along the entire length of the trench wall remain horizontal except near to the main fault zone, indicating that the dominant slip component is strike-slip. However, there is some evidence of secondary-order normal component of deformation distributed within a zone of about 4 m along ruptures dipping southwest (Fig. 17). The main difference between sites 1 and 2 is the situation of the bedrock. Within the T1bis and T1 trenches, the Miocene-Pliocene bedrock is located south of the main fault zone while at site 2 the bedrock is situated on the northern side of the fault trace. This observation is characteristic of displaced topographies and/or key beds along steep strike-slip fault planes with variable dip-directions.

23

In such a case, the secondary vertical component of faulting, and the orientation of the uplifted block, could vary along the fault trace.

5.3. Dating analysis

To determine the chronology of the identified paleoearthquakes within the trench walls of site 1, eight samples were collected for optical stimulated luminescence (OSL) analysis. The objective of OSL dating method is to determine the time elapsed since the last exposure of quartz-rich sandy sediments to sufficient sunlight. The results of dating analysis, which performed in OSL dating laboratory of the Quebec University are summarized in Table 2. The age of the sampled units varies from 12.4 kyr to 51.8 kyr. All the ages are consistent with the stratigraphic order units and define a relatively wide time window. Due to lack of organic materials for radio carbon dating and the lack of suitable quartz rich sediments for OSL analysis the upper most units were not dated in T1bis and T1 trenches (units 5, 6a, and 6b).

Hereafter, to interpret the paleoseismic events, we discuss more specifically the recognized seismites on the trench walls. To identify the paleoearthquakes that ruptured the east-central sector of the TFS, we focused our analysis on site 1 and especially within the T1bis and T1 trenches. Our decision was influenced by the uncertainties associated with the interpretation of unit geometries in T3 trench (site 2) and the available OSL ages. To constrain the paleoearthquake chronology, we reconstructed the geometric and sedimentary evolution of the fault zone (Figs. 15 and 18A–F). The illustration presented in Fig. 15 shows the situation after the oldest identified strong earthquake within the T1bis and T1 trenches. The erosion surface between the units 1 and 2 corresponds to the event horizon of this paleoearthquake. Unit 2b is a colluvial wedge, lateral equivalent to unit 2a, which together can be interpreted as the post-event horizon for one or stack of several seismic events. In the T1bis and T1

trenches, sample TL T1bis.3 (51.8±5 Kyr) defines the minimum possible age of the oldest earthquake. The observed liquefaction features within unit 2a (Figs. 12, 13, and 14) implies that at least one large seismic event took place during the sag pond sedimentation (24.5–51.8 kyr at minimum). The following evolutions are presented in Figs. 18A–F:

Fig. 18A shows the situation at the time of the surface faulting associated with the second strong earthquake. Unit 2b and its lateral equivalent (unit 2a) represent the event horizon of this paleoearthquake.

Fig. 18B shows an erosion stage that occurred after the second paleoearthquake. The basal portion of unit 3 (33.5±3 kyr), which covers the erosion surface, is interpreted as the post-event horizon of the second detected earthquake.

Fig. 18C shows the sedimentation of unit 4 before the occurrence of third paleoearthquake. The base of this unit yields an age of 12.4±1 kyr.

Fig. 18D shows the restoration of the ground surface to its position just after the penultimate strong earthquake. The top of unit 4 (ground surface) corresponds to the event horizon of this third paleoearthquake.

Fig. 18E shows the erosion surface that affected the top of units 2a and 4, and the deposition of units 5 and 6 that formed after the third paleoearthquake.

Fig. 18F shows the situation during the most recent surface faulting event, which can be associated with the 1721 AD earthquake as it affected the uppermost soils situated close to the surface. The exception is the presence of a discontinuous veneer of soil that corresponds to the present-day ground surface and has been developed during the last 300 years (see paleoseismological logs in Figs. 12 and 13).

We also found a seismic event within the T2 trench with an age older than 18.5±2 kyr (unit 5 is the post-event horizon) that could be associated with one of the oldest seismic events recognized within the T1bis and T1 trenches. Within the T2 trench, a younger event (<18.5±2 kyr) cuts unit 5 and is overlain by unit 6 (corresponding to the last post-event horizon). This last earthquake could be considered as the penultimate or the most recent seismic event (the 1721 AD earthquake) recognized in the T1bis and T1 trenches.

6. Discussion and conclusion

The NTF belongs to a regional fault system, the TFS, which extends over 300 km. The TFS together with the GSKF system form a mainly right-lateral crustal fault network (Guilato-Siahcheshmeh-Khoy-Tabriz; GSKT fault network) extending to the northwest over 600 km (Fig. 1). This fault network also includes E-striking oblique-slip, reverse-dextral and N-striking normal fault segments which are compatible with a regional N–S compression.

Our observations indicate that the maximum cumulative horizontal (dextral strike-slip) Pliocene-Quaternary offsets on the TFS evolves along the three sectors of the fault system: the NW, Central, and SE sectors, from about 800 and 300 m in the west- and east-central portions to a few meters in the western and eastern fault terminations. This distribution pattern is explained by the occurrence of crustal shortening in the Mishu and Bozghush ranges at the both ends of the NW and SE fault segments of the NTF. In other words, the two west- and east-central sectors correspond to right-lateral strike-slip fault segments of the NTF. The western and eastern ends of the TFS contain oblique-slip, reverse-dextral and dip-slip reverse faults. These fault terminations correspond to compressional fault relay zones that

accommodated a significant part of the horizontal displacements along the North Tabriz strike-slip fault. Such a deformation pattern indicates a transpressional tectonic regime. Along the TFS, normal faulting appears to be limited only to local deformation within the overlapping zones between right-step fault segments and branches of the dextral NTF as well as to local extrado deformation associated with large-scale folding in the Bozghush range.

The northern termination of the GSKT fault network has a horsetail geometry composed of N–S normal faults associated with numerous active volcanoes. The southeastern termination, in NW Iran, is mainly characterized by an active compressional tectonic regime, which is limited to the Bozghush range (Fig. 1). These features strongly suggest that the Bozghush range is not only the eastern termination of the TFS but also corresponds to the SE end of the GSKT fault network. The GSKT fault network defines a transcurrent fault system that is situated between two opposite extensional and compressional tectonic regimes at its both ends. This kinematic model is consistent with the N–S direction of convergence between the Arabian and Eurasian plates. This also implies that the NTF is totally independent of the North Anatolian fault, contrary to that proposed earlier by some authors (Westaway, 1990; Jackson et al., 1992).

The maximum Pliocene-Quaternary cumulative right-lateral geomorphic offset (~800 m) along the NW segment of the NTF is more than twice that of the SE segment (~300 m). Paleoseismological trenching performed along the east-central sector of the fault system (the SE segment of the NTF) revealed the occurrence of at least three strong seismic events during the last 33.5 kyr. Hessami et al. (2003a) have shown that the west-central sector of the fault system (the NW segment of the NTF) experienced a much higher rate of strain release, with four large seismic events in the last 3.6 kyr. This could explain the differences in the coseismic slip rates and earthquake characteristics of the two fault segments. This eastward decrease in slip rate could imply a more distributed fault zone along the SE segment of the

fault. As shown in section 4.2 and illustrated in figures 2, 4, and 6, the SE segment of the NTF contains numerous parallel branches and right-stepped strands, defining a wider fault zone than the NW segment of the fault. This NW segment contains narrower deformation zone dominated by dextral movements, which are associated with reverse component. It seems that a large part of deformation along the SE segment of the fault is accommodated by right stepping, which results in lateral spreading of faulting. This wider deformation zone along the SE segment of the NTF, along with its kinematics (e.g. normal dip-slip component of faulting that has been mostly localized within right-stepped overlap zones) could imply a more distributed fault zone. In fact, the vertical component of the slip vector along the southeastern sector of the NTF is a little more than along the NW segment of the fault. This diffuse deformation could also imply smaller Pliocene-Quaternary cumulative dextral offsets and slower seismic deformation along the SE segment of the fault than along the NW segment. Our results exclude the earlier hypothesis of a spatially constant slip rate along the NTF (e.g. Masson et al., 2006; Rizza et al., 2013).

To explain the apparent geomorphologic, kinematic, and seismologic differences between the NW and SE segments of the NTF within the southeastern termination zone of the GSKT fault network, the following characteristics can be inferred.

Indeed, the spatial change in the long-term slip rate of the NTF could explain why the Pliocene-Quaternary geomorphic offsets are smaller in the SE segment and why deformation is more distributed (the fault zone is less mature in the southeast). In addition, the earthquakes rupturing the SE segment have stronger (M~7.7) magnitudes, hence longer return periods, than those occurring on the NW segment of the NTF (M~7.5). This feature could be also related to differences in the fault segment geometry (length and second-order segmentation) or due to the variations of fault-friction properties along the fault; possibly caused by the presence of the Sahand volcano along the SE segment (Fig. 1). Moreover, the larger mean

value of ~7 m for the smallest dextral displacements measured along the SE segment, in compare to ~4.5 m for the NW segment, agrees with this inference. The longer return periods relate to only strong earthquakes along the SE segment of the NTF but not moderate seismic events, which have logically shorter return periods and already threaten Tabriz city and its surrounding areas.

According to the available seismic records, the coseismic slip rate along the NTF is not constant on a short time scale, and it is mainly controlled by earthquake clustering as proposed earlier by Berberian (1997) and Karakhanian et al. (2004). In this model, paleoseismological records for the SE segment of NTF might be missing some strong seismic events if they occurred close in time to each other. In such cases, insufficient time would have elapsed for any differentiated post-event horizons to be formed, especially during dry and cold climate periods. In other words, one identified seismic event in the paleoseismological data could correspond to two or more strong earthquakes that occurred during a short time period. All these considerations highlight the differences in seismic behavior and, particularly, in coseismic slip rate variations along the NW and SE segments of the NTF.

Complementary paleoseismological records along the TFS, especially within its western and eastern termination zones, are still needed to complete the seismic behavior and kinematics of the individual fault segments over the Late Pleistocene and Holocene time scales; both of them are essential in the assessment of the regional seismic hazard.

References

Ambraseys, N., 1978, The relocation of epicentres in Iran, *Geophys. J. R. astr. Soc.*, 53, 117–121.

Ambraseys, N. and Melville, C. P., 1982, *A history of Persian earthquakes*, Cambridge Earth Science Series, Cambridge University Press, London.

Avagyan, A., 2001, Estimation of slip rates and recurrence intervals of strong earthquakes on the fault system of Pambak-Sevan-Sunik (Armenia): Segmentation and relation with volcanic activity, PhD thesis, Montpellier II University, France.

Barka, A. A., and Kadinsky-Cade, K., 1988, Strike-slip fault geometry in Turkey and its influence on earthquake activity. *Tectonics*, 7(3), 663–684.

Barka, A. A., 1992, The North Anatolian fault, *Annales Tectonicae*, 6, 164–195.

Berberian, M., and Arshadi, S., 1976, On the evidence of the youngest activity of the North Tabriz fault and the seismicity of Tabriz city, *Geol. Surv. Iran Rep.,* 39, 397–418.

Berberian, M., 1981, Active faulting and tectonics of Iran. In H. K. Gupta and F. M. Delaney (Eds.), *Zagros-HinduKush-Himalaya Geodynamic Evolution*, American Geographical Union, Washington, DC, pp: 33–69.

Berberian, M., 1994, Natural hazards and the first earthquake catalog of Iran, vol. 1: *Historical hazards in Iran prior 1900*, I.I.E.E.S. report.

Berberian, M., 1995, Master "blind" thrust faults hidden under the Zagros folds: Active basement tectonics and surface morphotectonics. *Tectonophysics*, 241, 193–224.

Berberian, M., 1997, Seismic sources of the Transcaucasian historical earthquakes. In S. Giardini and Balassanian, S. (Eds.), *Historical and prehistorical earthquakes in the Caucasus*. Kluwer Academic Publishing, Dordrecht, Netherlands, pp. 233–311.

Berberian, M., and Yeats, R. S., 1999, Patterns of historical earthquake rupture in the Iranian plateau, *Bull. Seismol. Soc. Am.*, 89, 120–139.

Bertero, V., Frohmberg, K., Gath, E., Greene, M., Hays, W., Power, M., Youd, T. L., 1994, Liquefaction, Earthquake Basics Brief No. 1, Free publication of Earthquake Engineering Research Institute (EERI), USA, 8P.

Cisternas, A. and Philip, H., 1997, Seismotectonics of the Mediterranean region and the Caucasus. In D. Giardini and S. Balassanian (Eds.), *Historical and prehistorical earthquakes in the Caucasus*. Kluwer Academic Publishing, Dordrecht, Netherlands, pp. 39–77.

Copley, A., and Jackson, J., 2006, Active tectonics of the Turkish-Iranian Plateau, *Tectonics*, 25, TC6006, doi: 10.1029/2005TC001906.

Davtyan, Vahan, 2007, Les faille actives d'Arménie; estimation des vitesses de déplacement par la géodésie (GPS), l'archéosismologie et la paléosismologie, PhD thesis, université Montpellier 2, France.

Eftekhar Nezhad, J., 1975, Brief history and structural development of Azarbaijan. *Geological Survey of Iran*, Internal Report, 8P.

Eftekhar Nezhad, J., 1993, Geology map of Tabriz 1:100 000, Geological Survey of Iran, Tehran, Iran.

Fathian Baneh, A., Solaymani Azad, S., Nazari, H., Ghorashi, M., and Talebian, M., 2011, Preliminary results of new paleoseismological investigations along the North Tabriz fault. Paper presented at the International Union of Geodesy and Geophysics (IUGG) General Assembly, Melbourne, Australia, 28 June–7 July.

Foroutan, M., M. Sébrier, H. Nazari, B. Meyer, M. Fattahi, A. Rashidi, K. Le Dortz, and M. D. Bateman (2012), New evidence for large earthquakes on the Central Iran plateau: Palaeoseismology of the Anar fault, *Geophys. J. Int.*, *189*(1), 6–18, doi:10.1111/j.1365-246X.2012.05365.x.

Foroutan, M., Meyer, B., Sébrier, M., Nazari, H., Murray, A. S., Le Dortz, K., Shokri, M. A., Arnold, M., Aumaître, G., Bourlès, D., Keddadouche, K., Solaymani Azad, S., and M. J. Bolourchi (2014), Late Pleistocene-Holocene right slip rate and paleoseismology of the Nayband fault, western margin of the Lut block, Iran, *J. Geophys. Res. Solid Earth*, *119*(4), 3517-3560.

Forte, A.M., Cowgill, E., Bernardin, T., Kreylos, O., Hamann, B., 2010, Late Cenozoic deformation of the Kura fold-thrust belt, southern Greater Caucasus, Bulletin of Geological Society of America, 122 (3/4); p. 465-486; doi: 10.1130/B26464.1.

Frankel, K. L. and J. F. Dolan, 2007. Characterizing arid region alluvial fan surface roughness with airborne laser swath mapping digital topographic data. J. Geophys. Res., 112, F02025, doi:10.1029/2006JF000644.

Hempton, M. R., and Dewey, J. F., 1983, Earthquake-induced deformational structures in young lacustrine sediments, East Anatolian fault, southeast Turkey. *Tectonophysics*, 98, 7–14.

Hessami, K., Pantosi, D., Tabassi, H., Shabanian, E., Abbassi, M-R., Feghhi, K., and Solaymani, S., 2003, Paleoearthquakes and slip rates of the North Tabriz fault, NW Iran: Preliminary results, *Ann. Geophys*. 46, 903–915.

Hessami, K., Jamali, F., and Tabassi, H., 2003, Map of major active faults of Iran, International Institute of Earthquake Engineering and Seismology.

Hessami, K., and Jamali, F., 2008, New evidence of earthquake faulting in Tabriz city, NW Iran, *Geoscience,* 17, 1, 156–161.

Ishihara, K., 2006, Liquefaction of subsurface soils during earthquakes; 1974, Journal of Disaster Research, 1 (2), 245-261.

Jackson, J., 1992, Partitioning of strike-slip and convergent motion between Eurasia and Arabia in Eastern Turkey and the Caucasus, *J. Geophys. Res.*, 97, 12471–12479.

Jackson, J., and McKenzie, D. 1984, Active tectonics of the Alpine-Himalayan Belt between western Turkey and Pakistan, Geophysical Journal of the Royal Astronomical Society, 77 (1), 185–264.

Jackson, J.A. & Ambraseys, N.N., 1997, Convergence between Eurasia and Arabia in eastern Turkey and the Caucasus, in Historical and Prehistorical Earthquakes in the Caucasus, pp. 79–90, eds Giardini, D. & Balassanian, S., Kluwer Academic Publishers, Dordrecht.

Jackson, J., Priestley, K., Allen, M., and Berberian, M., 2002, Active tectonics of the South Caspian Basin. *Geophysical Journal International*, 148, 214–245.

Kagan, Y. Y., and Jackson, D. D., 1991, Long-term earthquake clustering, *Geophys. J. Int.*, 104, 117–133.

Karakhanian, A., Djrbashian, R., Trifonov, V., Philip, H., Arakelian, S., and Avagian, A., 2002, Holocene-historical volcanism and active faults as natural risk factor for Armenia and adjacent countries. *J. Volcanol. Geotherm. Res.*, 113 (1–2), 319–344.

Karakhanian, A., Jrbashyan, R., Trifonov, V., Philip, H., Avagyan, A., Hessami, K., Jamali, Bayraktutan, F. M., Bagdassarian, H., Arakelian, S., Davtyan V., and Adilkhanyan, A., 2004, Active faulting and natural hazards in Armenia, eastern Turkey and Northern Iran, *Tectonophysics*, 380, 189–219.

Le Dortz, K., Meyer, B., Sébrier, M., Braucher, R., Nazari, H., Benedetti, L., Fattahi, M., Bourlès, D., Foroutan, M., Siame, L., Rashidi, A., and M. D. Bateman (2011), Dating inset terraces and offset fans along the Dehshir Fault (Iran) combining cosmogenic and OSL methods, Geophys. J. Int., 185, 1147-1174.

Maggi, A., Jackson, J. A., Priestley, K., and Baker, C., 2000, A re-assessment of focal depth distributions in southern Iran, the Tien Shan and Northern India: Do earthquakes really occur in the continental mantle? *Geophys. J. Int.*, 143, 629–661.

Masson, F., Djamour, Y., van Gorp, S., Chéry, J., Tatar, M., Tavakoli, F., Nankali, H., and Vernant, P., 2006, Extension in NW Iran driven by motion of the South Caspian Basin, *Earth Planet. Sc. Lett.*, 252, 180–188.

Meghraoui, M., Ersen Aksoy, M., Serdar Akyuz, H., Ferry, M., Dikbas, A., and Altunel, E., 2012, Paleoseismology of North Anatolian fault at Guzelkoy (Ganos Segment, Turkey): Size and recurrence time of earthquake ruptures west of the Sea Marmara, *Geoche. Geophys. Geosyst.*, 13(4), Q04005, doi: 10.1029/2011GC003960.

Nabavi, M. H., 1976. Preface to geology of Iran, *Geological survey of Iran*, p. 109 (in Persian).

Nilforoushan, F., Masson, F., Vernant, P., Vigny, C., Martinod, J., Abbassi, M-R., Nankali, H., Hatzfeld, D., Bayer, R., Tavakoli, F., Ashtiani, M., Doerflinger, E., Daignières, M., Collard, P., and Chéry, J., 2003, GPS network monitors the Arabia–Eurasia collision deformation in Iran, J. Geody., 77, 411–422.

Nissen, E., Tatar, M., Jackson, J., and M. B. Allen, 2011, New views on earthquake faulting in the Zagros fold-and-thrust belt of Iran, Geophys. J. Int., 186, 928-944, doi:10.1111/j.1365-246X.2011.5119.x.

Oveisi, B., Lav´e, J., van der Beek, P., Carcaillet, J., Benedetti, L., and Aubourg, C., 2008, Thick- and thin-skinned deformation rates in the central Zagros simple folded zone (Iran) indicated by displacement of geomorphic surfaces*, Geophys. J. Int.*, 176, 627–654.

Philip, H., Cisternas, A., Gvishiani, A., and, Gorshkov, A., 1989, The Caucasus: An actual example of the initial stages of continental collision, *Tectonophysics*, 161, 1–21.

Philip, H., Avagyan, A., Karakhanian, A., Ritz, J.-F., and Rebai, S., 2001, Estimating slip rates and recurrence intervals for strong earthquakes along an intracontinental fault: Example of the Pambak-Sevan-Sunik fault (Armenia), *Tectonophysics*, 343, 205–232.

Priestley, K., Baker, C., and Jackson, J., 1994, Implications of earthquake focal mechanism data for the active tectonics of the South Caspian Basin and surrounding regions, *Geophys. J. Int.*, 118, 111–141.

Reilinger, R. E., McClusky, S., Vernant, P., Lawrence, S., Ergintav, S., Cakmak, R., Ozener, H., Kadirov, F., Guliev, I., Stepanyan, R., Nadariya, M., Hahubia, G., Mahmoud, S., Sakr, K., ArRajehi, A., Paradissis, D., Al-Aydrus, A., Prilepin, M., Guseva, T., Evren, E., Dimitrotsa. A., Filikov, S. V., Gomez, F., Al-Ghazzi, R. and Karam, G., 2006, GPS

constraints on continental deformation in the Africa- Arabia-Eurasia continental collision zone and implications for the dynamics of plate interactions, J. Geophys. Res., 111, B05411, doi: 10.1029/ 2005JB004051.

Rizza, M., Vernant, P., Ritz, J.-F., Peyret, M., Nankali, H., Nazari, H., Djamour, Y., Salamati, R., Tavakoli, F., Chery, J., Mahan, S.-A., and Masson, F., 2013, Morphotectonic and geodetic evidence for a constant slip-rate over the last 45 kyr along the Tabriz fault (Iran), *Geophys. J. Int.*, 193, 1083–1094, doi: 10.1093/gji/ggt041.

Rockwell, T., Ragona, D., Seitz, G., Landgridge, R., Aksoy, M. E., Ucarkus, G., Ferry, M., Meltzner, A., J., Klinger, Y., Meghraoui, M., Satir, D., Barka, A., and B. Akbalik, 2009, Palaeoseismology of the North Anatolian Fault near the Marmara Sea: implications for segmentation and seismic hazard, in *Palaeoseismology: Historical and Prehistorical Records of Earthquake Ground Effects for Seismic Hazard Assessment*, edited by Reicherter, K., Michetti, A. M., and P. G. Silva, *Geol. Soc. Lond. Spec. Publ.*, 316, 31–54.

Sengör, A. M. C., and Kidd, W. S. F., 1979, Post-collisional tectonics of the Turkish-Iranian plateau and a comparison with Tibet. *Tectonophysics*, 55, 361–376.

Şengör, A. M. C., and Yilmaz, Y., 1981, Tethyan evolution of Turkey: A plate tectonic approach, *Tectonophysics*, 75, 181–241.

Shabanian, E., Bellier, O., Siame, L., Abbassi, M. R., Bourlès, D., Braucher, R., and Y. Farbod (2012), The Binalud Mountains: A key piece for the geodynamic puzzle of NE Iran, Tectonics, 31, TC6003, doi:10.1029/2012TC003183.

Siahkali Moradi, A., 2008. Seismicity-seismotectonic and velocity structure of the earth's crust within the Bam and Tabriz strike-slip fault zones, PhD thesis, International Institute of Earthquake Engineering and Seismology (IIEES).

Siahkali Moradi, A., Hatzfeld, D., and Tatat, M., 2011, Microseismicity and seismotectonics of the North Tabriz fault (Iran), *Tectonophysics*, 506, 22–30.

Solaymani Azad, S., 2009, Evaluation de l'aléa sismique pour les villes de Téhéran, Tabriz et Zandjan dans le NW de l'Iran, Approche morphotectonique et paléosismologique, PhD thesis, University of Montpellier (in French and English).

Solaymani Azad, S., Dominguez, S., Philip, H., Hessami, K., Foroutan, M., Shahpasand Zadeh, M., Ritz, and J.-F., 2011, The Zandjan fault system: Morphological and tectonic evidence of a new active fault network in the NW of Iran, *Tectonophysics*, 506, 73–85.

Stöcklin, J., 1968, Structural history and tectonics of Iran: A review. *American Association of Petroleum Geologists Bulletin* 52, 1229–1258.

Stöcklin, J., 1974, Mesozoic-Cenozoic orogenic belts: Data for orogenic studies. In: A. Spencer (Ed.), *Northern Iran: Alborz Mountains*. Geological Society Special Publication, London, vol. 4, pp. 213–234.

Tatar, M., Hatzfeld, D., and Ghafory-Ashtiany, M., 2004, Tectonics of the central Zagros (Iran) deduced from microearthquake seismicity, *Geophys. J. Int.*, 156, 255–266.

Talebian, M., and Jackson, J., 2004, A reappraisal of earthquake focal mechanisms and active shortening in the Zagros mountains of Iran, *Geophys. J. Int.*, 156, 506–526.

Vernant, P., Nilforoushan, F., Hatzfeld, D., Abbassi, M.-R., Vigny, C., Masson, F., Nankali, H., Martinod, J., Ashtiani, A., Bayer, R., Tavakoli, F., and Chéry, J., 2004, Contemporary crustal deformation and plate kinematics in Middle East constrained by GPS measurement in Iran and northern Oman, *Geophys. J. Int.*, 157, 381–398.

Vernant, P., and Chéry, J., 2006, Low fault friction in Iran implies localized deformation for the Arabia-Eurasia collision zone, *Earth Planet. Sci. Lett.*, 246, 197–206.

Wells, D. L., and Coppersmith, K. J. (1994), New empirical relationships among magnitude, rupture length, rupture width, rupture area, and surface displacement, *Bull. Seismol. Soc. Am.*, 84, 974–1002.

Westaway, R., 1990, Seismicity and tectonic deformation rate in Soviet Armenia: Implications for local earthquake hazard and evolution of adjacent regions, Tectonics, 9, 477–503.

Figure Caption:

Fig.1. Active tectonic map showing the general pattern of recent deformation in the north-central portion of the Arabia–Eurasia collision zone and the situation of the North Tabriz fault (NTF) within the NW Iran-Transcaucasian region. Right- and left-lateral strike-slip faulting occurs along the NW and NE fault trends, respectively. Fold and thrust belts and normal faulting, associated with active volcanoes, revealed active N–S compression and E–W extension (see text for details). The instrumental seismicity (yellow circles) is from the Incorporated Research Institutions for Seismology (IRIS). The black and gray focal-mechanisms are respectively from Jackson et al. (2002) and USGS. GPS arrows are from Reilinger et al. (2006). The historical seismicity is from Berberian (1997) and Ambraseys and Melville (1982). The pointed lines show the active fold axis. GSKF: Guilato-Siahcheshmeh-Khoy fault system; NAF: North Anatolian fault; CF: Chalderan fault; AKF: Akurian fault; MF: Maku fault; TF: Tassuj fault; SaF: Salmas fault; GF: Garni fault; PSSF: Pambak-Sevan-Sunik fault; WCF: West Caspian fault; AF: Astara fault; TF: Talesh fault; ZF: Zandjan fault (Solaymani Azad et al., 2011).

Fig.2. In recent centuries, five successive and destructive seismic events have occurred along the TFS at Sarab (1593 AD), SE Tabriz (1721 AD), NW Tabriz (1780 AD), Marand (1786 AD), and Tassuj (1807 AD). This seismic sequence, spanning a period of 214 years, started from the SE termination of the TFS and propagated toward its NW end. Note the E–W trending active folding (pointed line) west of the Marand city. 1: Tassuj fault; 2: North Mishu fault; 3: South Mishu fault; 4: Sufian fault; 5: Shabestar fault; 6: NW segment of the NTF; 7: SE segment of the NTF; 8: Duzduzan fault; 9: South Sarab fault; 10: North Bozghush fault; 11: South Bozghush fault. The historical seismicity is from Ambraseys and Melville (1982), Berberian (1997) and Berberian and Yeats (1999). The positions of Figs. 3, 4, 5, and 7 are marked by gray rectangles. The meizoseismal areas of the 1721 AD and 1780 AD events denote the outline of Fig. 4.

Fig.3. SPOT Satellite image of the west of Marand city. A large E–W trending Quaternary fold (amplitude ~100 m), formed as a result of active N–S shortening, shows a clear antecedent stream pattern (see Fig. 2 for location). Southwest of the fold, a main dextral strike-slip fault (the North Mishu fault), situated in the prolongation of the NTF, and clearly offsets the drainage network. The coexistence of ~E–W trending Quaternary folding and

N110°E active strike-slip faulting reveals slip partitioning and confirms that the tectonic regime is mainly transpressive along this portion of the TFS.

Fig.4. Landsat 7 satellite image of the Tabriz region and its tectonic interpretation (see Fig. 2 for location). The limits of the 50 km long NW and 60 km long SE segments of the NTF are represented respectively by black-filled and empty triangles. These NW and SE fault segments bound the southern flank of the Mero range and the northern flank of the Sahand volcano, respectively. Tabriz city is situated in the overlap zone of about 15 km between these two segments of the NTF in a large pull-apart basin. The SE segment of the NTF, which constitutes the east-central part of the TFS, exhibits several right-stepped fault branches and a wider fault zone compared to the NW segment of the fault, which constitutes the west-central part of the fault system.

Fig.5. (left) Near the Khajeh-Marjan village (see Fig. 4 for location), the NW segment of the NTF crosscuts several generations of alluvial fans (the chronological classification is based on down-cutting erosion). Zone 0 represents the bedrock and the alluvial fans are labeled from oldest (zone 1) to youngest (zone 3). The observed maximum cumulative right-lateral offset of the alluvial fans is about 500 m. (right) Farther to the east, a 800 m horizontal morphologic offset is also observable and can be reconstructed by fitting the main drainage network on both sides of the fault. This offset represents the greatest measured cumulative offset (through the Pliocene-Quaternary units) along the whole fault segment.

Fig.6. (a) Aerial photograph and (b) morphotectonic interpretation of the two right-stepped en-echelon branches of the SE segment of the NTF that bound the Ghurugol lake (see Fig. 4 for location). Based on these observations, Ghurugol lake can be interpreted as a small pull-apart basin formed in response to right-lateral strike-slip movements along the fault branches. Furthermore, the drainage pattern on both sides of the lake shows a paleostream direction toward the northeast. The northeastern catchment associated with the lake evolved recently, possibly due to the fault activity inducing uplift of the northern compartment of the fault. On the eastern side of the lake, several right-lateral, strike-slip offset features show evidence of repeated coseismic surface faulting (stream beds 1, 2, 3, and 4) accrued through the past earthquakes. The mean value of the largest observable cumulative dextral offset of the four stream beds along this part of the TFS is approximately 300 m. East of the lake, three parallel fault branches labeled as branches I, II, and III reveal a wider fault zone than the NW segment

of the NTF (see text for details). (c) Index map. (d) SE segment of the NTF. View to the east of the main fault plane west of Ghurugol lake (between Shebli and the lake in Fig. 4). At this location, the fault cuts through a Quaternary colluvium (on the northern side), abutting against the Miocene-Pliocene bedrock (to the southern side). The mean value of measured dextral striations associated with normal component at this location is N145°E, 65° N, 22° SE (fault slip data: strike, dip/dip-direction, and rake, respectively). (e) Outcrop of the northern fault branch of the NTF zone (branch I in Fig. 6b) east of Ghurugol lake (looking south). In this area, the deformed zone is composed of two parallel hairline surface ruptures trending parallel to the range. These faults cut the ground surface indicating recent active faulting.

Fig.7. Morphostructural map and simplified N–S cross-section of the eastern end of the TFS within the Bozghush range (see Fig. 2 for location). A large portion of the strike-slip component of the NTF is accommodated along the several oblique reverse faults, mainly E–W trending, and an extrados extension located at the top of the Bozghush range antiform. As in the Marand region (Fig. 3), slip partitioning in a transpressive tectonic regime can be evidenced. Alluvial surfaces, with slopes less than 2°, are colored as a function of their relative altitude (rainbow-color scale) to highlight topographic offsets related to active faulting.

Fig.8. Offset reconstruction (a$_o$) and morphostructural interpretation (a) of satellite imagery (b) and perspective view (looking northeast) of the trench sites (c) along the NTF, east of Ghurugol lake (see Figs. 6a and 6b for location). The NTF zone crosscuts several streambeds incised within the Quaternary alluvial fans covering the range piedmont (made of the Eocene volcanics) parallel to the fault trace. The southern part of these alluvial fans is dammed by several hills associated with large shutter ridges. Gray polygons in Fig. 8a mark a shuttered hill (made of the Eocene igneous rocks) formed by cumulative dextral offset. The two red arrows in Fig. 8c show the fault trace. Note the Quaternary strike-slip faulting features such as beheaded drainages and dextral offset streams (~300 m). These features make the region a suitable site to perform paleoseismological studies. T1, T1bis, T2, and T3 delineate trench locations at sites 1 and 2.

Fig.9. Evidence of recent right-lateral offsets along the SE segment of the NTF in the vicinity of sites 1 and 2. (a) Small ridge, located 200 m southeast of T1 trench, is dextrally offset by 7±2 m. The piercing points are marked by black arrows at the both sides of the fault trace

(white dashed line). (b) Clear right-lateral offset drainage (7±1 m) observed along the SE segment of the NTF between T3 trench and Bostanabad. The small amplitude of stream bed incision (2–3 m) reveals that the offset occurred recently, most probably during the most recent strong earthquake that ruptured this segment of the NTF.

Fig.10. Field photos (top and middle) and schematic cross-section (bottom) showing the structure and geometry of the deformed Miocene-Pliocene bedrock (M-Pl) and Pliocene-Quaternary fan deposits (Pl-Q) at the trench site 1. The faults that bound both sides of the hill have affected Late Quaternary deposits (LQ). The dashed rectangular boxes indicate the location of the trenches. The blue solid line shows the ground surface level. See text for details.

Fig.11. Detailed topographic map based on a digital elevation model (DEM) extracted from differential global positioning system (DGPS) surveying of the trench site 1. Structural interpretation is based on field observations (see Fig. 8 for location). Note two (T1bis and T1) and one (T2) trenches that have been excavated across the main dextral fault and the secondary thrust fault trace, respectively.

Fig.12. East wall of T1bis trench across the main fault zone at site 1 (see Figs. 8, 10, and 11 for location); rectified photo mosaic of the trench wall (top). To minimize geometric distortions and perform accurate measurements, each photo has been orthorectified using the Envi 4.3 software package. This new technique provides a very good comparison between the photo mosaics and the trench logs. (bottom) Paleoseismological log of the T1bis trench. Labeled dots locate the OSL samples. During the past large seismic events, the bedrock (to the south) was sheared and thrusted over younger soil and colluvium units (to the north). See text for details.

Fig.13. West wall of T1 trench across the main fault zone at site 1 (see Figs. 8, 10, and 11 for location). (top) Rectified photo mosaic of the trench wall. (bottom) The trench log and dating sampling locations. See section 5.1.1 for details.

Fig.14. The flame-form distribution of liquefaction features in sandy-silty materials of unit 2a within T1bis trench (looking east). See Fig. 12 for location, between meters 0 and 4.

Fig.15. Reconstruction of the main sedimentary unit geometries after the oldest paleoevent found in T1bis and T1 trenches. The schematic cross-section shows that these fault ruptures were sealed by the deposition of units 2a and 2b.

Fig.16. (top) Field photograph looking southeast of T2 trench. (bottom) Paleoseismological log and the dating sampling locations of the T2 trench at site 1. This trench was excavated across a NE-dipping thrust fault located just southwest of T1 and T1bis trenches (see Fig. 11). The surface rupture associated with this fault is clearly visible in the morphology and in the aerial photos and can be followed for several hundred meters toward the southeast (see Figs. 8, 10, and 11 for location).

Fig.17. (top) View of the T3 trench across the NTF at site 2. The narrow and steep shear zone of the main right-lateral strike-slip deformation separates Pliocene-Quaternary alluvial fan deposits (to the south) and Miocene-Pliocene (M-Pl) bedrock and its Late Quaternary cover (to the north). (bottom) The trench log and dating sampling locations. The width of the fault zone is about 5 m close to the surface and less than 2 m at a depth of about 5 m. The right-lateral strike-slip faulting was concentrated at depth in a narrow zone (between meters 1.8A and 2.1A). Near the surface, the fault zone becomes wider (between meters 1.0F and 5.0F). Some evidence of a normal component has been preserved on a few fault planes located at an intermediate depth (between meters 3B and 4B, i.e., N137°E, 75° SW).

Fig.18. Schematic cross-sections show the chronological stages of coseismic surface rupturing events and their recurrence-period situations after the first paleoevent (see Fig. 15) as recorded within T1bis and T1 trenches. See text for details.

Tables:

Table 1. Historical records for the Tabriz region (e.g. Ambraseys and Melville, 1982; Berberian 1997) reveal that since 858 AD this territory has experienced several destructive earthquakes. References are: (1) Ambraseys and Melville (1982), (2) Berberian (1994), (3) Berberian (1997).

Table 2. OSL dating results of important units in our paleoseismological trenches. See section 5.3 for details.
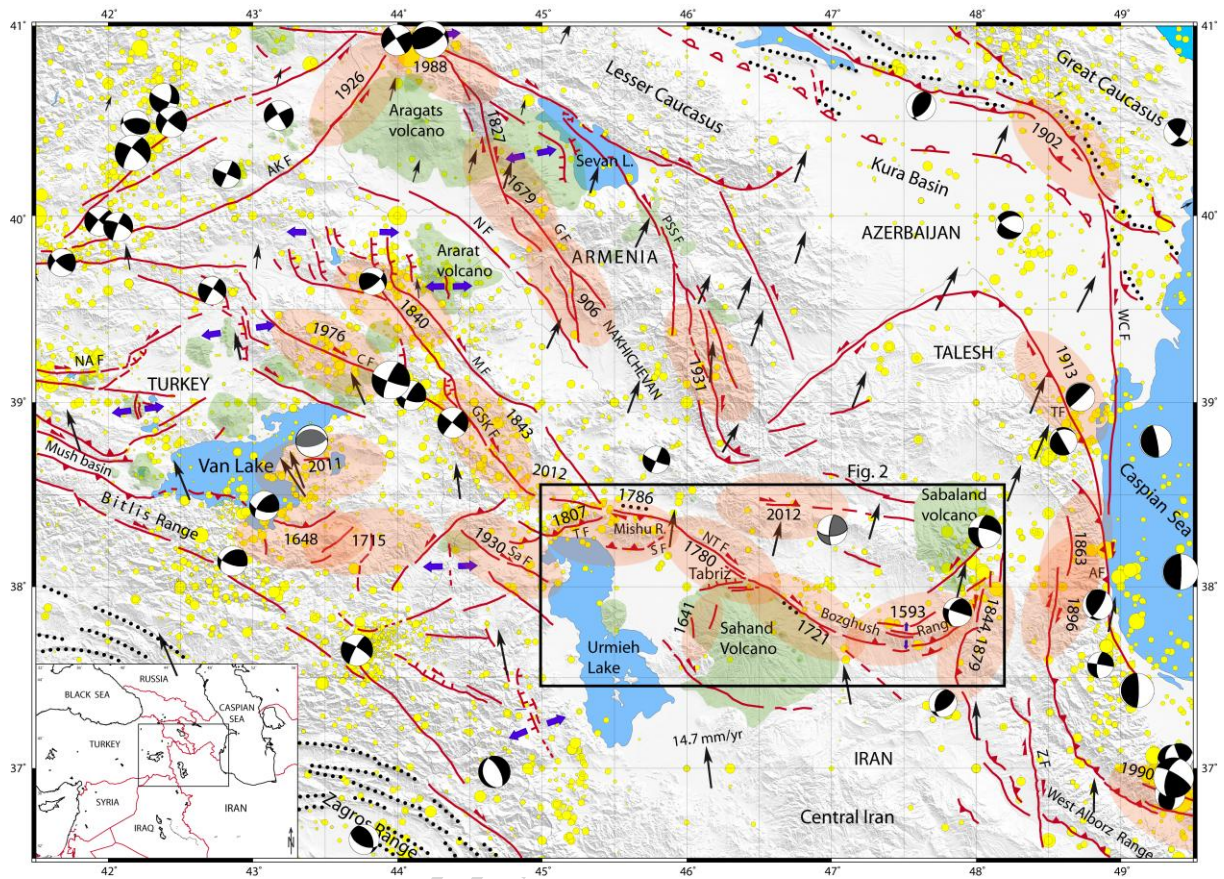
Figure 1
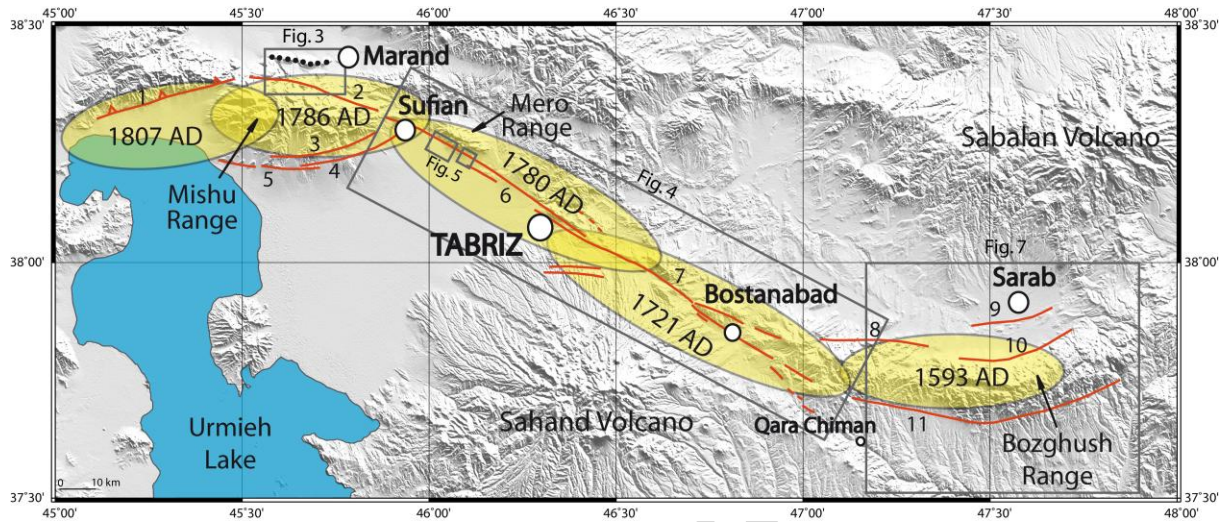
Figure 2
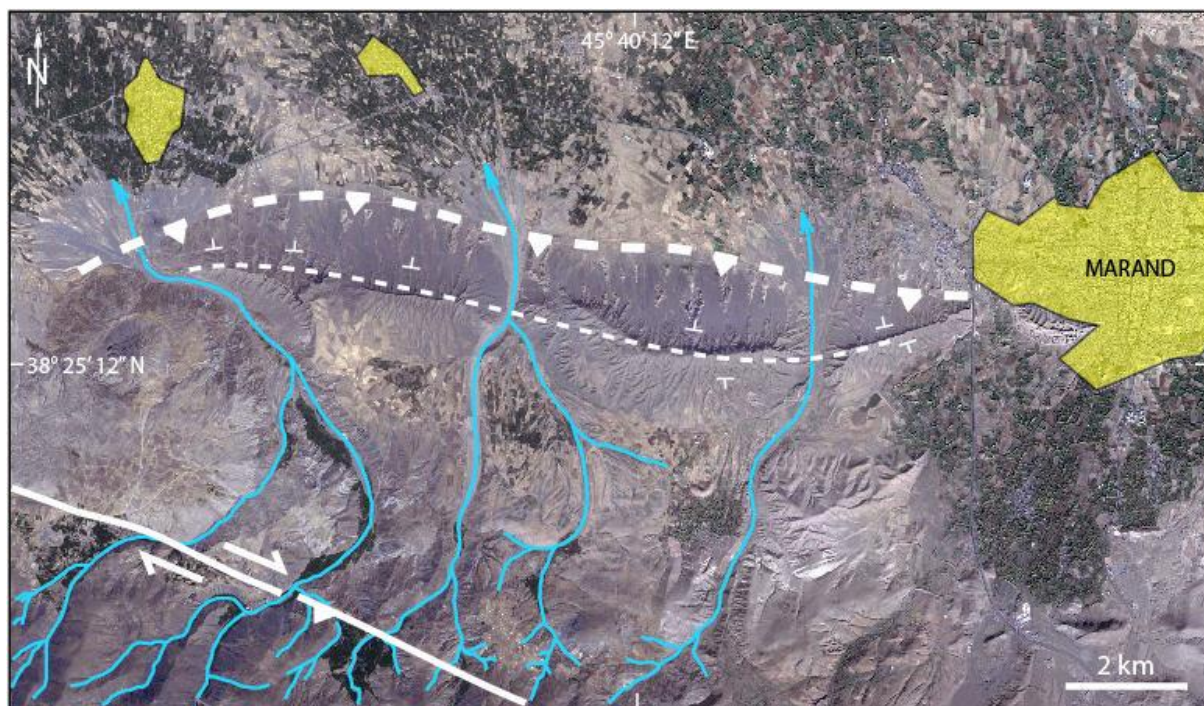
Figure 3
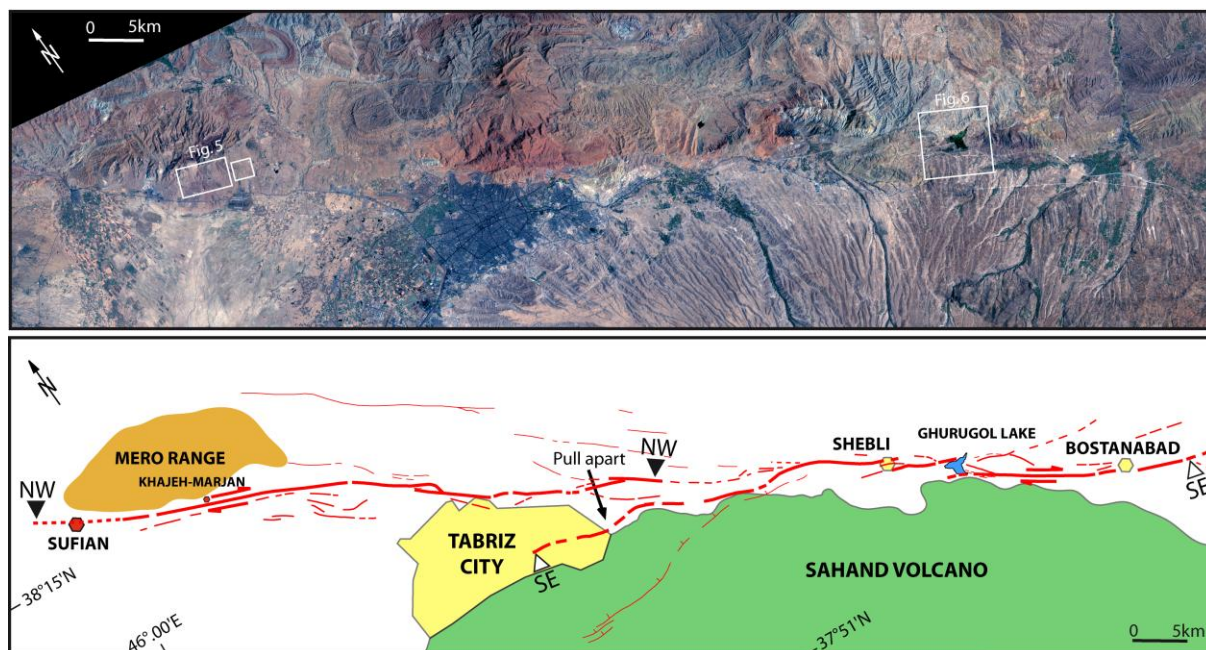
Figure 4
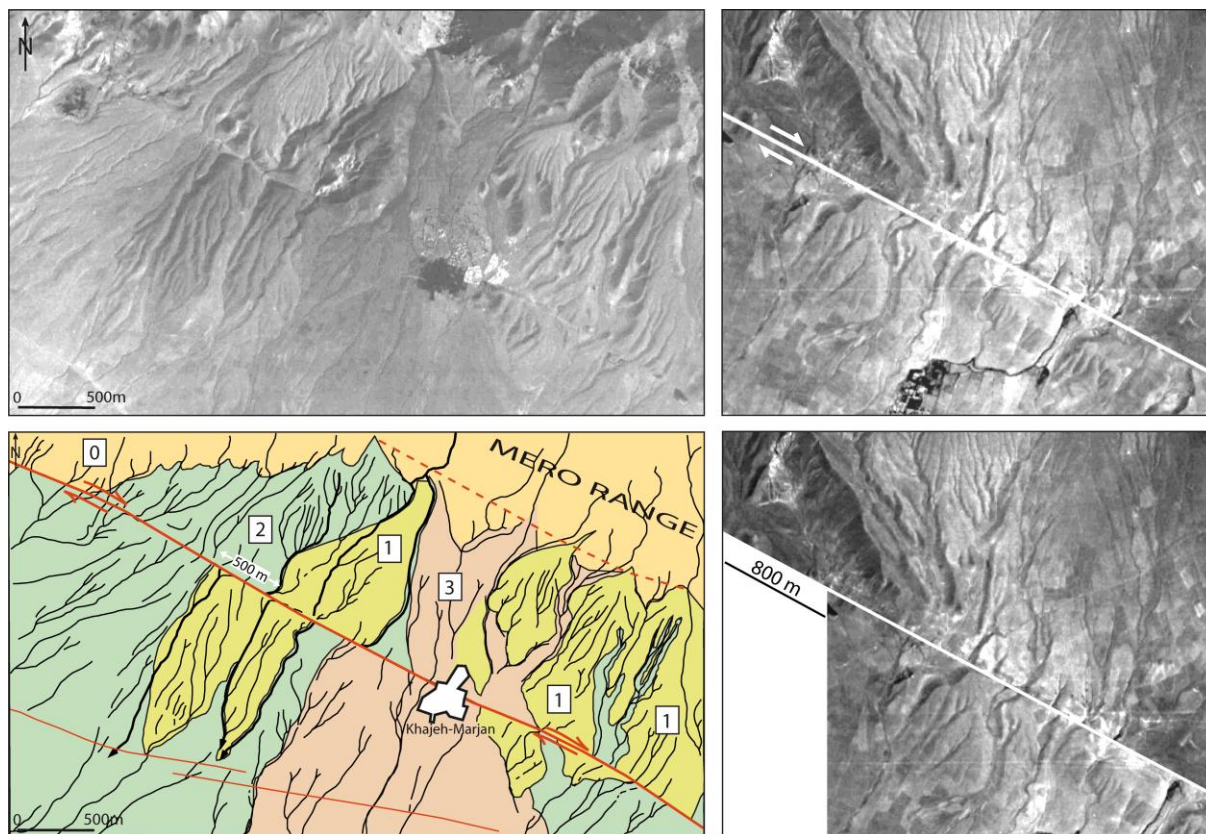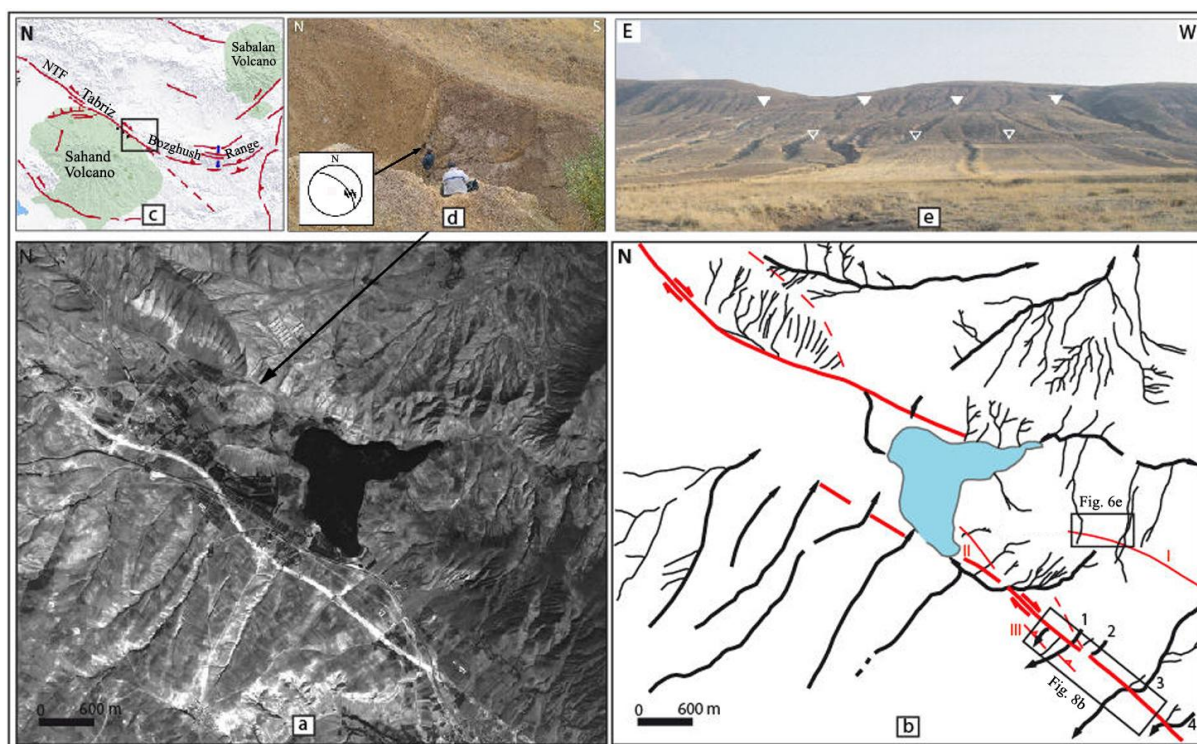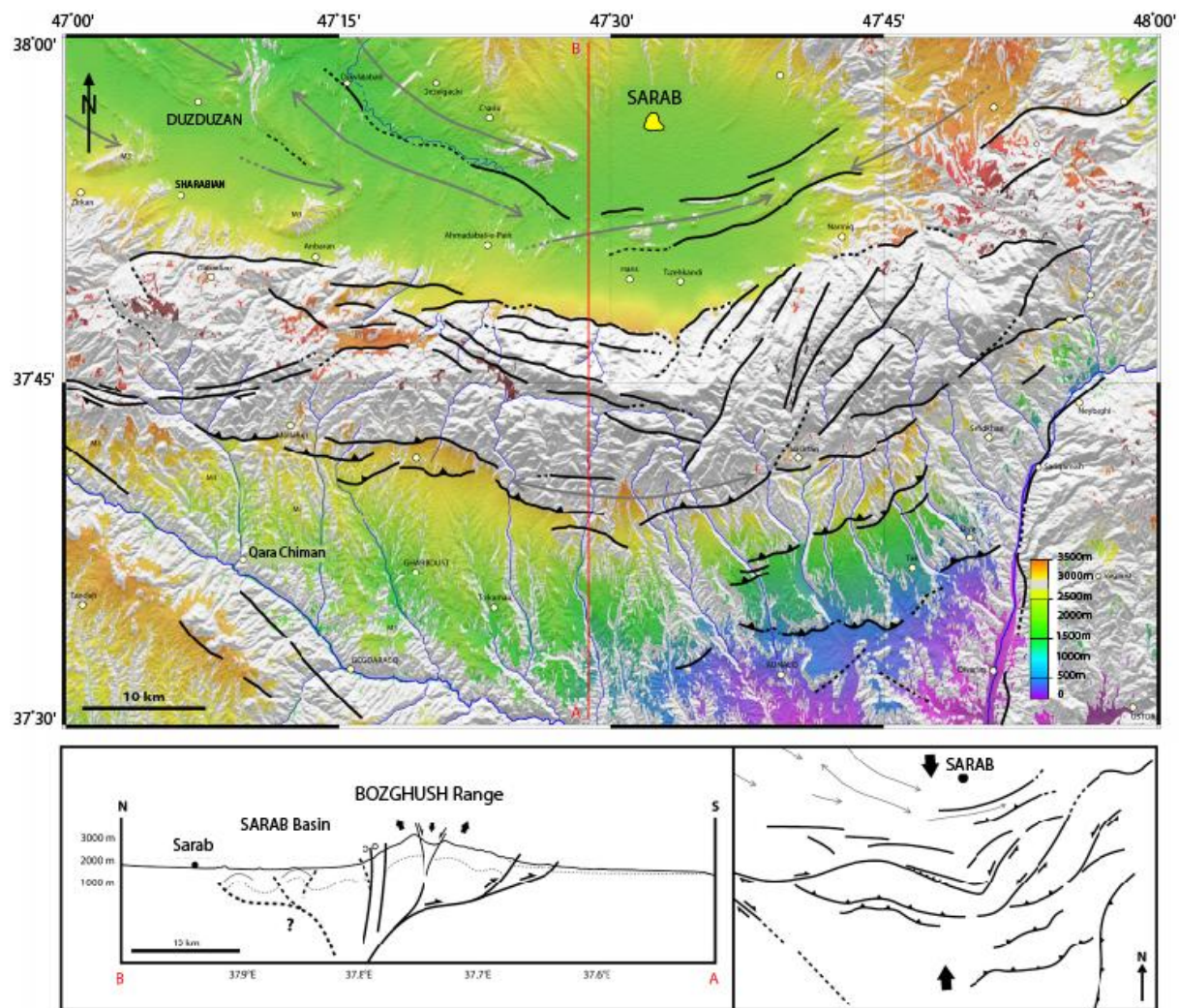
Figure 5

Figure 6

Figure 7
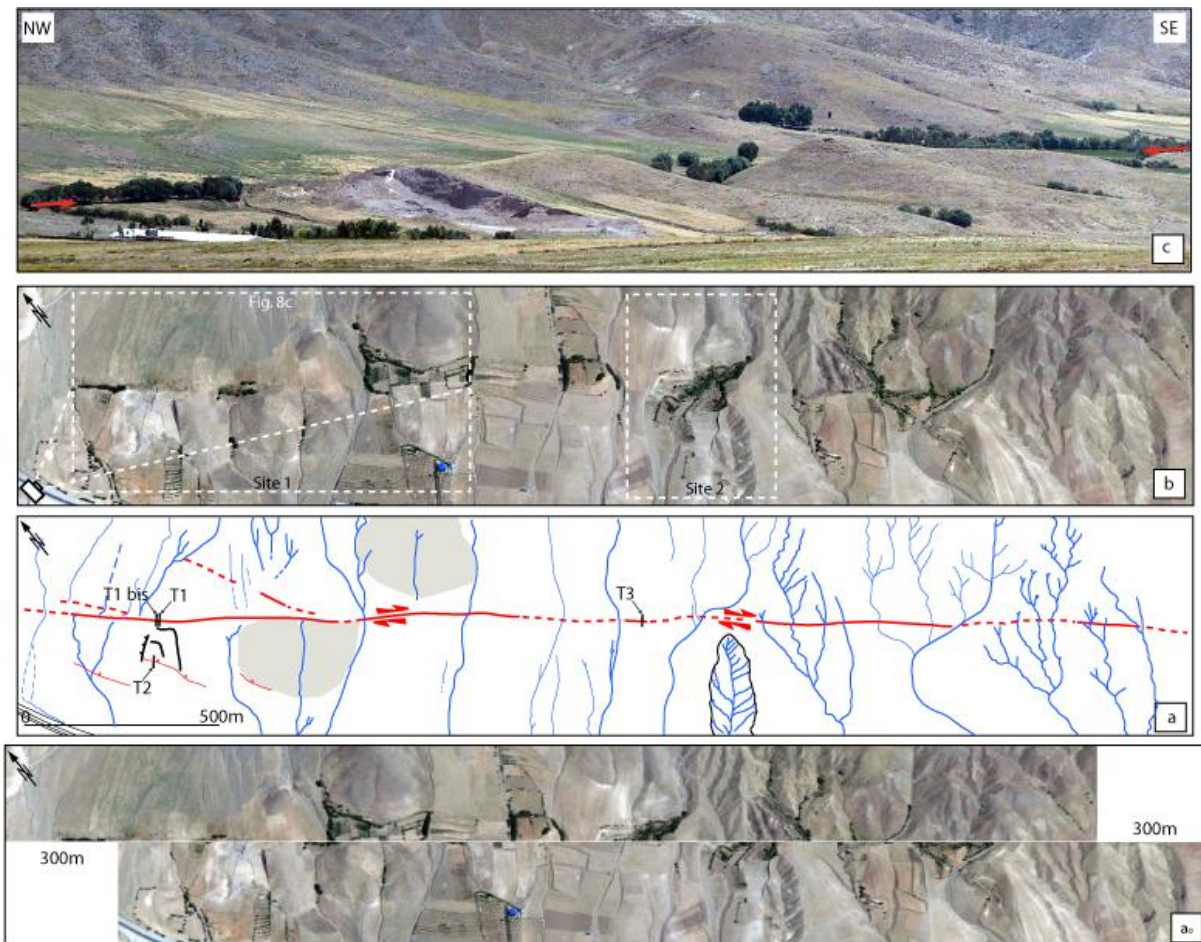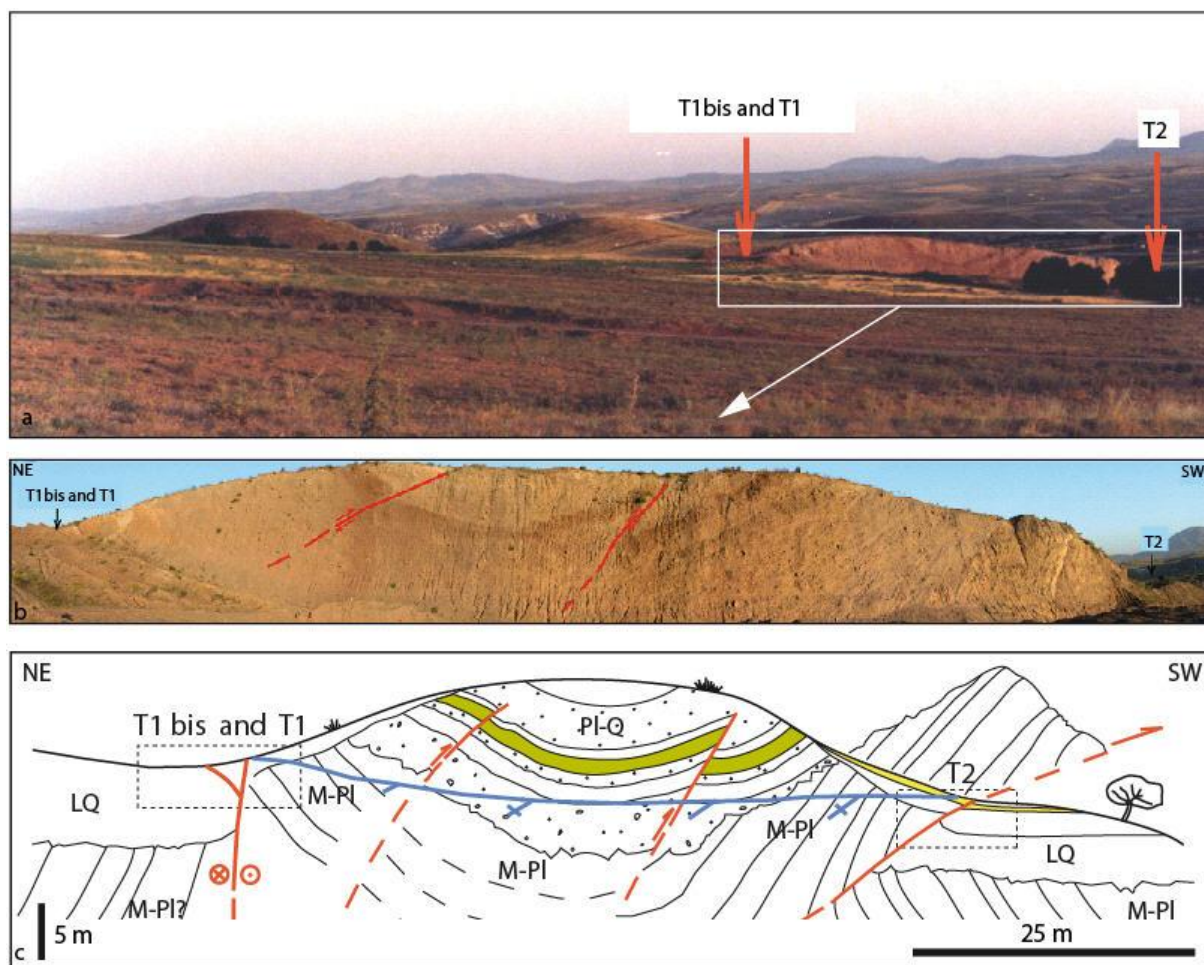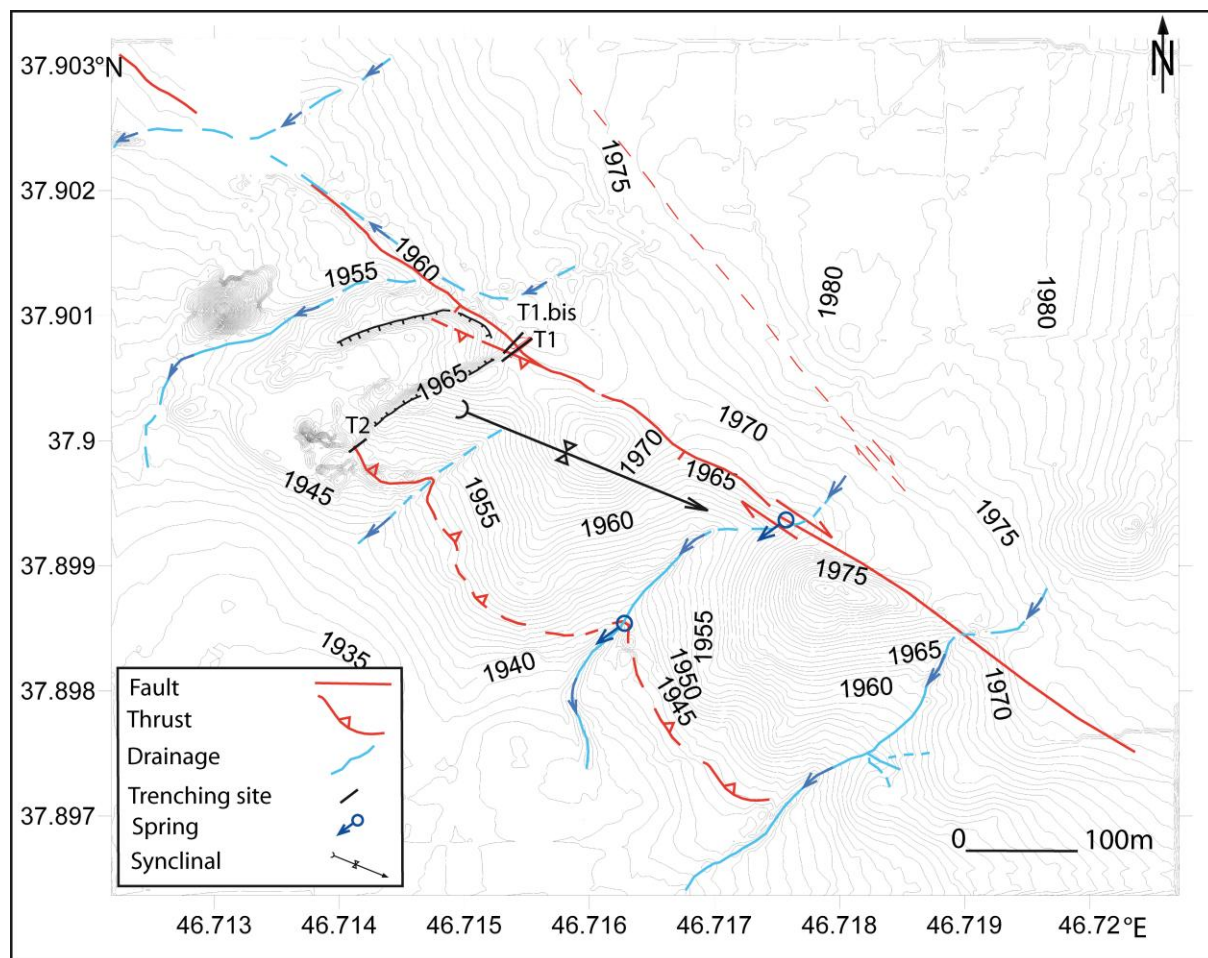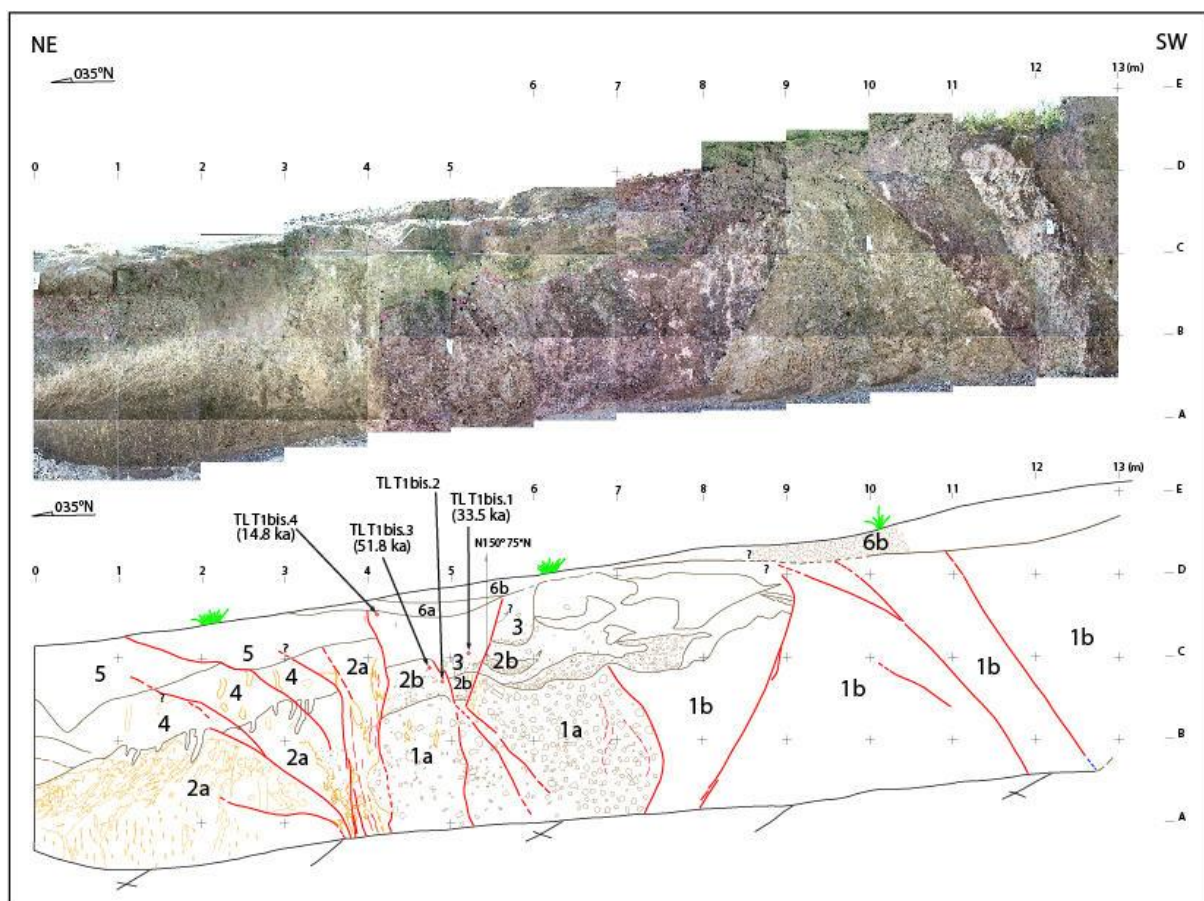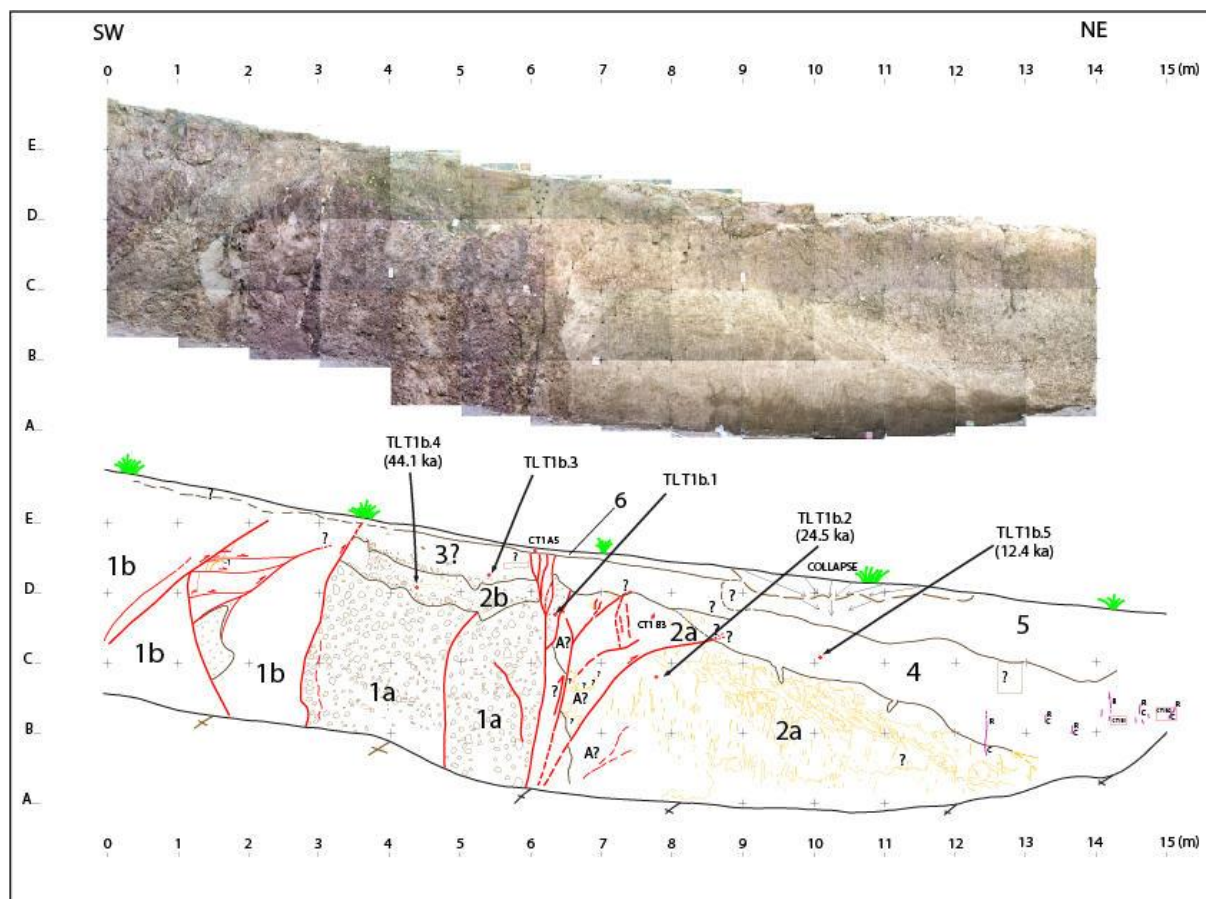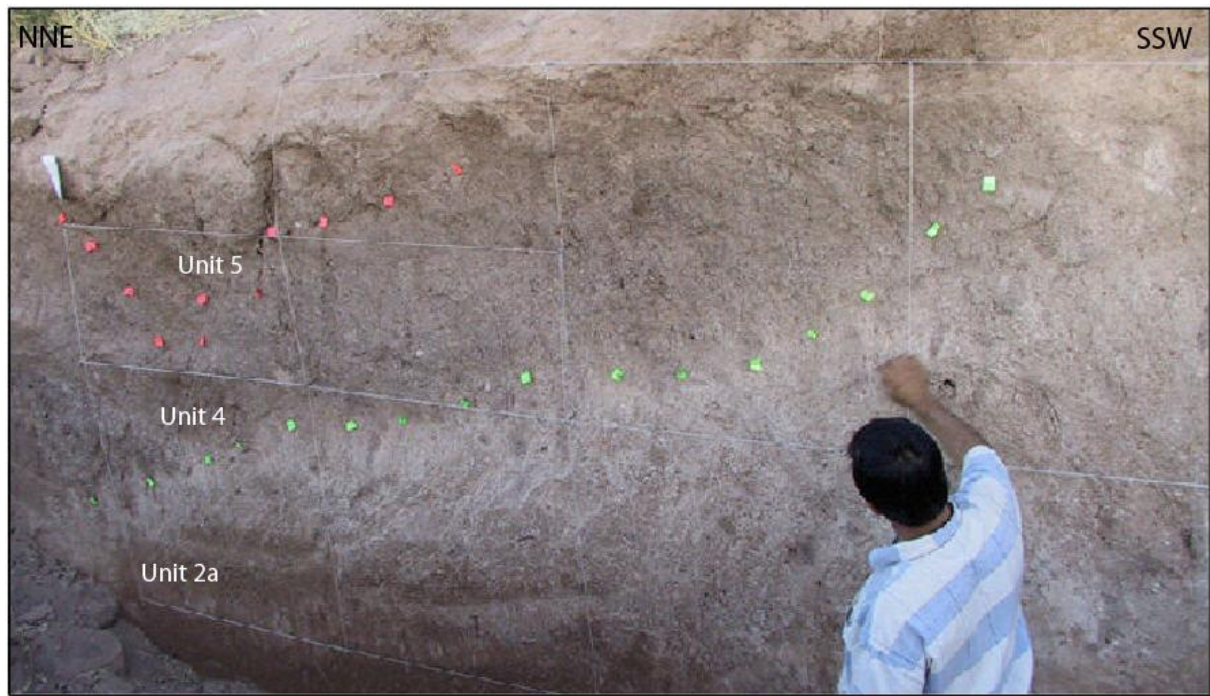
Figure 8

Figure 9

Figure 10
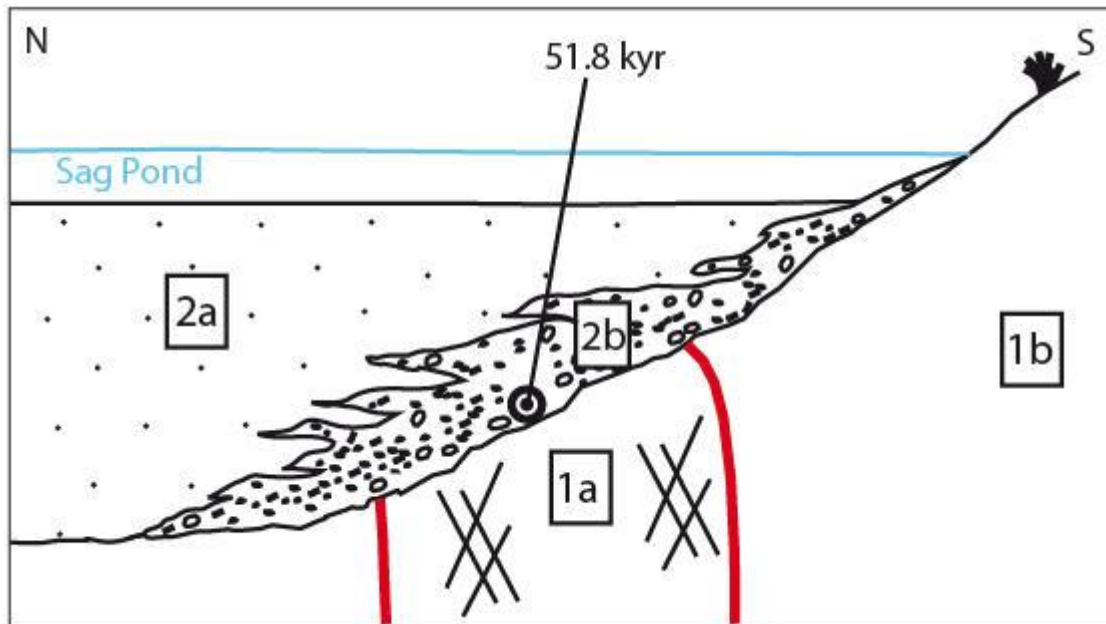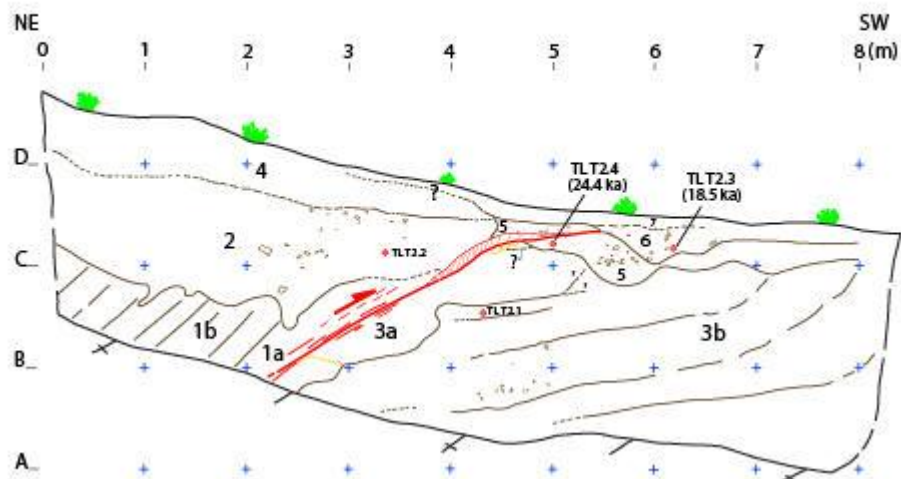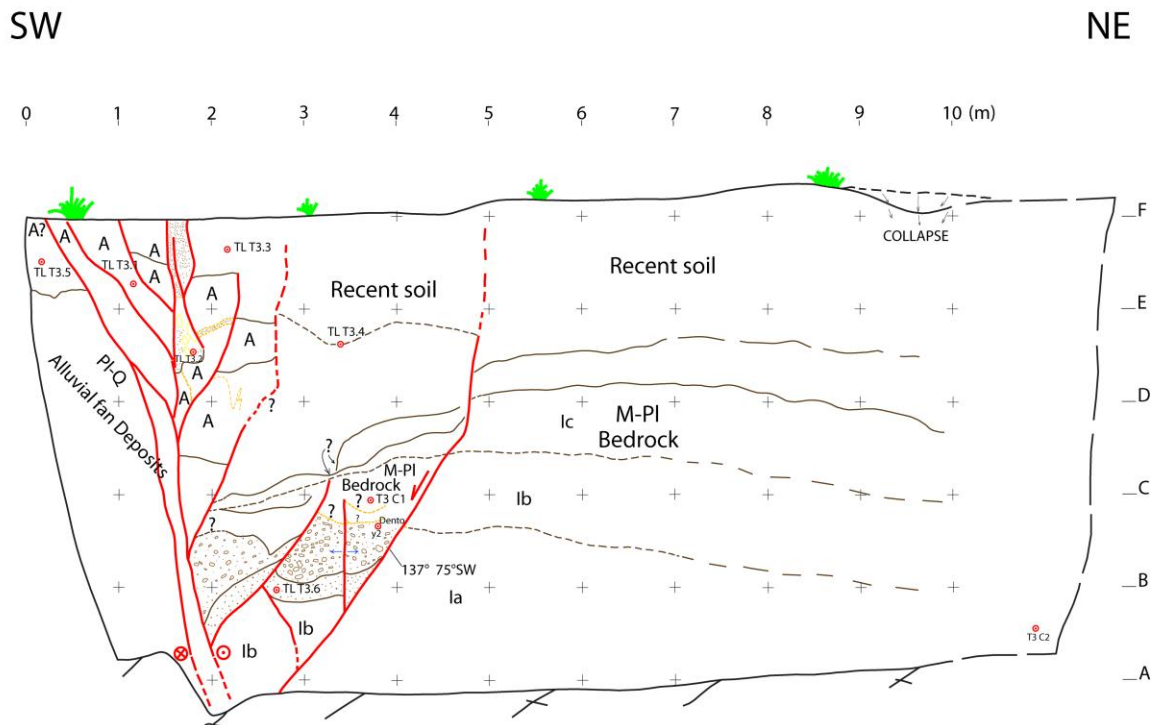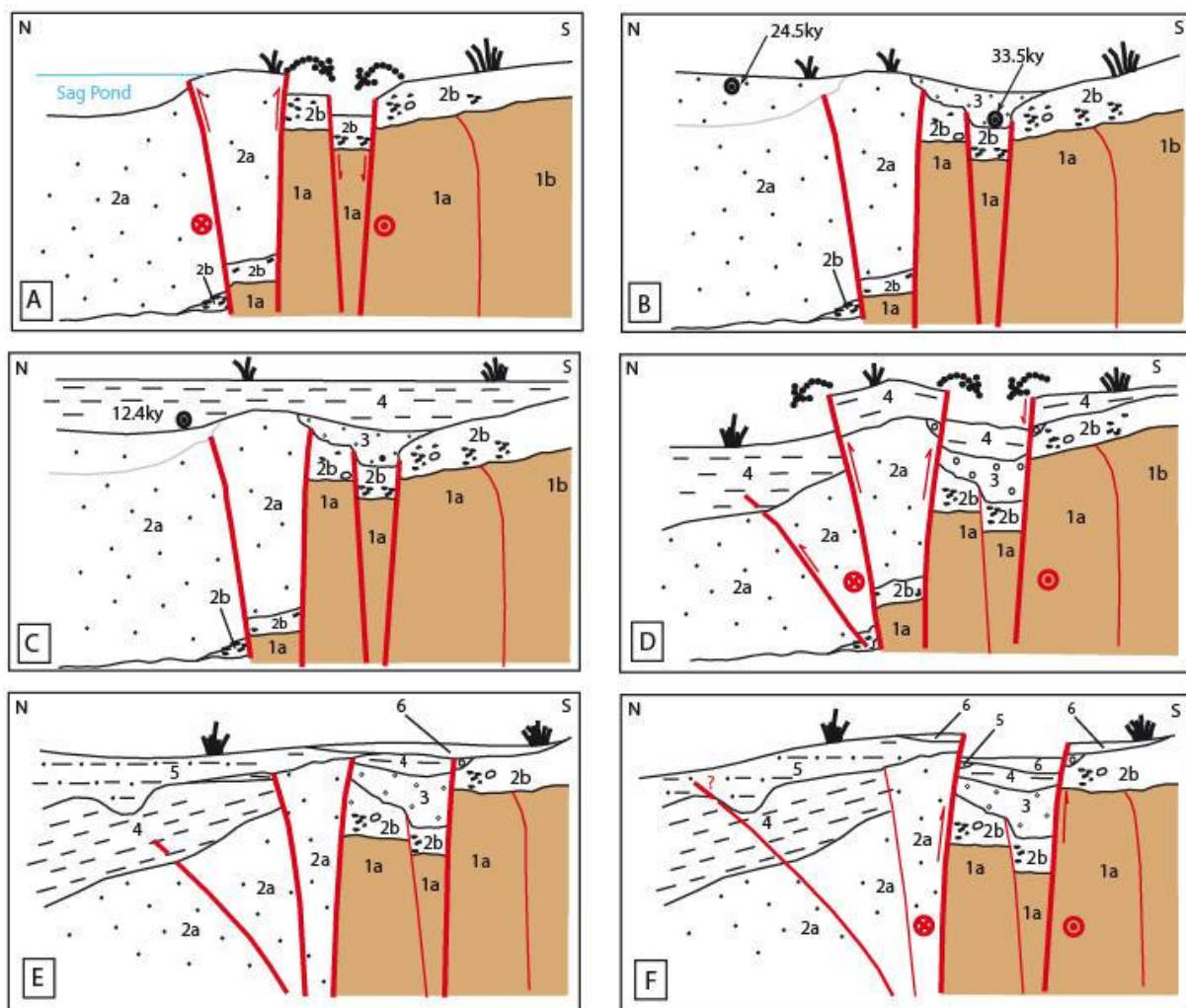
Figure 11

Figure 12

Figure 13

Figure 14

Figure 15

Figure 16

Figure 17

Figure 18

Table 1

Date of seismic event (AD)	Impact	Reference
858	Tabriz city was almost totally destroyed.	1
1042	Catastrophic earthquake occurred in Tabriz; 40,000 people were killed.	1, 3
1273	Large earthquake in Tabriz; 250 people were killed.	1
1345	Earthquake in Tabriz without causing damage.	1
1459	An Earthquake with large landslides was felt in Tabriz.	1
1550	A damaging earthquake caused many casualties and extensive landslides in the Tabriz region.	1
1624	A strong earthquake occurred in Tabriz but this is almost certainly a spurious event!	1, 3
1641	A destructive earthquake in the region between Tabriz and Urmieh lake occurred with great loss of life.	1, 2, 3
1650	An earthquake did much damage in Tabriz.	1
1717	An earthquake in Tabriz destroyed 4,000 houses; more than 700 people were killed.	1
1721	A major earthquake shook the Tabriz and SE region around it; more than 40,000 people were killed.	1, 2, 3
1780	A catastrophic earthquake occurred in the Tabriz region; over 200,000 people were perished.	1, 2, 3

Table 2

Sample No.	Trench No.	Unit	Age
TL-T1bis 1	T1.bis (east wall)	Base of 3	33.5 ka ± 10%
TL-T1bis 3	T1.bis (east wall)	top of 2b	51.8 ka ± 10%
TL-T1bis 4	T1.bis (east wall)	top of 3	14.8 ka ± 10%
TL-T1 b 2	T1 (west wall)	2a	24.5 ka ± 10%
TL-T1 b 4	T1 (west wall)	2b	44.1 ka ± 10%
TL-T1 b 5	T1 (west wall)	4	12.4 ka ± 10%
TL-T2-3	T2 (east wall)	6	18.5 ka ± 10%
TL-T2-4	T2 (east wall)	5	24.4 ka ± 10%

Highlights

- The SE segment of the NTF hosted successive earthquakes since the Late Quaternary

- Recent coseismic slip rate is decreasing along the NTF from the NW to the SE

- The SE segment of the NTF can be characterized by distributed coseismic deformation